

SOURCE
DATATRANSPARENT
PROCESSOPEN
ACCESS

Cilia-localized LKB1 regulates chemokine signaling, macrophage recruitment, and tissue homeostasis in the kidney

Amandine Viau^{1,2,3,†}, Frank Bienaime^{1,2,3,4,†}, Kamile Lukas¹, Abhijeet P Todkar¹, Manuel Knoll⁵, Toma A Yakulov^{1,2}, Alexis Hofherr^{1,2} , Oliver Kretz^{1,2,6,7}, Martin Helmstädter^{1,2}, Wilfried Reichardt^{2,8,9,10}, Simone Braeg¹, Tom Aschman⁵, Annette Merkle⁸, Dietmar Pfeifer^{2,11}, Verónica I Dumit¹², Marie-Claire Gubler^{13,14}, Roland Nitschke^{15,16}, Tobias B Huber^{1,2,7,16,17}, Fabiola Terzi³, Jörn Dengjel^{12,18} , Florian Grahhammer^{1,2,7}, Michael Köttgen^{1,2}, Hauke Busch^{9,10,19} , Melanie Boerries^{9,10,20}, Gerd Walz^{1,2,16}, Antigoni Triantafyllopoulou^{2,5,21} & E Wolfgang Kuehn^{1,2,16,*} 

Abstract

Polycystic kidney disease (PKD) and other renal ciliopathies are characterized by cysts, inflammation, and fibrosis. Cilia function as signaling centers, but a molecular link to inflammation in the kidney has not been established. Here, we show that cilia in renal epithelia activate chemokine signaling to recruit inflammatory cells. We identify a complex of the ciliary kinase LKB1 and several ciliopathy-related proteins including NPHP1 and PKD1. At homeostasis, this ciliary module suppresses expression of the chemokine CCL2 in tubular epithelial cells. Deletion of LKB1 or PKD1 in mouse renal tubules elevates CCL2 expression in a cell-autonomous manner and results in peritubular accumulation of CCR2⁺ mononuclear phagocytes, promoting a ciliopathy phenotype. Our findings establish an epithelial organelle, the cilium, as a gatekeeper of tissue immune cell numbers. This represents an unexpected disease mechanism for renal ciliopathies and establishes a new

model for how epithelial cells regulate immune cells to affect tissue homeostasis.

Keywords cilia; macrophages; nephronophthisis; polycystic kidney disease

Subject Categories Cell Adhesion, Polarity & Cytoskeleton; Immunology; Molecular Biology of Disease

DOI 10.15252/emj.201798615 | Received 9 November 2017 | Revised 13 May 2018 | Accepted 22 May 2018 | Published online 19 June 2018

The EMBO Journal (2018) 37: e98615

Introduction

Polycystic renal diseases belong to a spectrum of inherited disorders termed ciliopathies. They include genetically distinct and morphologically heterogeneous disorders that manifest at any time from early childhood to late in life and lead to end-stage kidney disease in

- 1 Renal Department, University Medical Center, Freiburg, Germany
 - 2 Faculty of Medicine, University of Freiburg, Freiburg, Germany
 - 3 INSERM U1151, Institut Necker Enfants Malades, Department of Growth and Signaling, Université Paris Descartes-Sorbonne Paris Cité, Paris, France
 - 4 Service d'Explorations Fonctionnelles, Hôpital Necker-Enfants Malades, Paris, France
 - 5 Department of Rheumatology and Clinical Immunology, University Medical Center, Freiburg, Germany
 - 6 Department of Neuroanatomy, Albert-Ludwigs-University Freiburg, Freiburg, Germany
 - 7 III. Department of Medicine, University Medical Center Hamburg-Eppendorf, Hamburg, Germany
 - 8 Medical Physics, Department of Radiology, and Comprehensive Cancer Center, University Medical Center, Freiburg, Germany
 - 9 German Cancer Consortium (DKTK), Freiburg, Germany
 - 10 German Cancer Research Center (DKFZ), Heidelberg, Germany
 - 11 Department of Hematology, Oncology and Stem Cell Transplantation, University Medical Center, Freiburg, Germany
 - 12 Center for Biological Systems Analysis (ZBSA), Core Facility Proteomics, Albert-Ludwigs-University Freiburg, Freiburg, Germany
 - 13 INSERM UMR1163, Laboratory of Inherited Kidney Diseases, Necker-Enfants Malades Hospital, Paris, France
 - 14 Imagine Institute, Université Paris Descartes-Sorbonne Paris Cité, Paris, France
 - 15 Center for Biological Systems Analysis (ZBSA), Life Imaging Center, Albert-Ludwigs-University Freiburg, Freiburg, Germany
 - 16 Center for Biological Signaling Studies (BIOSS), Albert-Ludwigs-University Freiburg, Freiburg, Germany
 - 17 Center for Biological Systems Analysis (ZBSA), Albert-Ludwigs-University Freiburg, Freiburg, Germany
 - 18 Department of Biology, University of Fribourg, Fribourg, Switzerland
 - 19 Institute of Experimental Dermatology, University of Lübeck, Lübeck, Germany
 - 20 Systems Biology of the Cellular Microenvironment Group, Institute of Molecular Medicine and Cell Research (IMMZ), Albert-Ludwigs-University, Freiburg, Germany
 - 21 Department of Rheumatology and Clinical Immunology, Charité - University Medical Centre Berlin, Berlin, Germany
- *Corresponding author. Tel: +49 761 270 32270; Fax: +49 761 270 32860; E-mail: wolfgang.kuehn@uniklinik-freiburg.de
[†]These authors contributed equally to this work

the majority of cases (Braun & Hildebrandt, 2016). In adults, they present as autosomal dominant polycystic kidney disease (ADPKD), one of the most common monogenetic disorders in man, with large numbers of cysts leading to massive enlargement of the kidneys (Ong et al, 2015). In children, the most prevalent form is nephronophthisis (NPHP). These kidneys are mostly small and fibrotic and contain only few cysts (Wolf, 2015; Konig et al, 2017). Important progress has been made in identifying the genetic causes of these entities: ADPKD is caused by mutations in either *PKD1* or *PKD2* (The International Polycystic Kidney Disease Consortium, 1995; Mochizuki et al, 1996). The number of *NPHP* genes has surpassed 20 and is growing annually (Hildebrandt et al, 1997; Saunier et al, 1997; Braun & Hildebrandt, 2016). Yet, very few insights exist into what links these diverse genes to the disease manifestations of cysts, inflammation, and fibrosis.

A key to this question lies in cilia, cell organelles that contain proteins mutated in the ciliopathies. Apart from kidney disease, ciliopathies also affect the liver, the central nervous system, and the skeleton (Hildebrandt et al, 2011). Motile cilia occur in bundles in the airways and brain, whereas primary cilia are non-motile filiform structures at the surface of most cell types, including renal tubules (Drummond, 2012). Cilia contain a microtubule-based cytoskeleton, an ultrastructural gate, and a complex macromolecular transport system (Nachury, 2014; Stepanek & Pigino, 2016; Garcia-Gonzalo & Reiter, 2017). They act as signal transducers receiving physical and chemical stimuli (Praetorius & Spring, 2001; Corbit et al, 2005; Lechtreck et al, 2009; Boehlke et al, 2010b) and affect a wide range of autonomous cellular functions such as cell size, polarity, cell cycle, and migration (Kim et al, 2004; Park et al, 2006; Robert et al, 2007; Jones et al, 2008; Vasilyev et al, 2009; Boehlke et al, 2010b; Schneider et al, 2010; Orhon et al, 2016). However, it is unclear how the dysfunction of cilia explains the phenotype of renal ciliopathies.

When exploring this question, two observations prompted our attention. First, apart from cysts, ADPKD and NPHP share an inflammatory phenotype: In NPHP, inflammation and subsequent fibrosis are much more prominent than cysts (Hildebrandt et al, 1997; Saunier et al, 1997; Wolf, 2015; Braun & Hildebrandt, 2016; Slaats et al, 2016). Likewise, in ADPKD macrophage infiltration occurs early on and promotes cyst enlargement (Karihaloo et al, 2011). Similarly to NPHP, the late stages of ADPKD are characterized by a severe degree of fibrosis (Norman, 2011; Ong et al, 2015).

The second aspect concerns the fact that metabolic signaling has been observed to contribute to ADPKD and NPHP (Chaki et al, 2012; Rowe et al, 2013; Menezes et al, 2016). We therefore asked the question how cilia, metabolic signal transducers, and inflammation are linked.

An interesting candidate to explore this question is the kinase liver kinase B1 (LKB1). Liver kinase B1 is a metabolic sensor localized in cilia (Boehlke et al, 2010b; Mick et al, 2015). We have previously shown *in vitro* that bending of cilia under flow activates LKB1 to phosphorylate its target AMPK (5'-adenosine monophosphate-activated protein kinase) at the base of cilia and to regulate metabolic signaling linked to PKD (Boehlke et al, 2010b; Walz et al, 2010; Liu et al, 2014; Orhon et al, 2016). To explore the role of LKB1 *in vivo*, we inactivated LKB1 in the kidney. First, we asked whether renal deletion of LKB1 induces a renal ciliopathy phenotype. Second, we sought to uncover molecular mechanisms connecting LKB1, cilia, and PKD proteins to cysts, inflammation, and fibrosis.

Results

Deletion of LKB1 in the kidney disrupts renal morphology and function

Mono-allelic mutations in the gene *STK11/LKB1* in humans cause Peutz-Jeghers disease, an inherited cancer syndrome characterized by benign tumors of the skin and intestine, as well as the development of malignancies (Hemminki et al, 1998). *Lkb1*^{-/-} mice display severe developmental defects leading to embryonic lethality. We therefore pursued a kidney-specific knockout strategy and crossed *Lkb1*^{flox/flox} mice (Nakada et al, 2010) with a kidney-specific deleter strain to excise *Lkb1* in the distal nephron. LKB1 was absent from the cilia of these tubule segments (*Lkb1*^{ATub}; Figs 1A and B, and EV1A–C), but the number and morphology of cilia were unchanged (Fig EV1D–F). The first sign of a renal disturbance was impaired urine concentration, which occurred at 5 weeks (Figs 1C and EV1G–I); magnetic resonance imaging (MRI) studies confirmed that increased amounts of urine were present in the renal pelvis and occasionally demonstrated a few cysts (Fig 1C). Macroscopically, the kidneys diminished in size over time (Fig EV1J and K; Appendix Fig S1). The occurrence of cysts was noted at the cortico-medullary

Figure 1. Loss of *Lkb1* in the mouse kidney disrupts renal architecture and causes inflammation and fibrosis.

- A LKB1 immunostaining in kidneys from control and *Lkb1*^{ATub} mice at 5 weeks. Representative images of *n* = 5 mice/group. Scale bars: 200 μ m. See also Fig EV1A and B.
- B Representative confocal microscopy images of collecting duct (CD, AQP2 expressing) from 5-week-old control (*n* = 4) and *Lkb1*^{ATub} (*n* = 5) animals. LKB1 is not expressed in CD primary cilia (Ac-Tub) of *Lkb1*^{ATub} mice. Scale bars: 2 μ m. See also Fig EV1C.
- C Magnetic resonance tomography images obtained at 10 and 16 weeks. Representative images of coronal kidney sections of *n* = 3 mice/group at 10 weeks (control) and *n* = 8 (*Lkb1*^{ATub}) at 16 weeks. Scale bars: 2 mm. See also Appendix Fig S1A.
- D Plasma blood urea nitrogen (BUN) at 5, 14, and 23 weeks (w).
- E Kaplan–Meier survival curves of control (*n* = 13) and *Lkb1*^{ATub} (*n* = 15) mice.
- F Periodic acid–Schiff (PAS) staining from control (5 weeks) and *Lkb1*^{ATub} mice at 5, 14, and 23 weeks. Arrowheads indicate cysts. *Lkb1*^{ATub} mice: representative of *n* = 13 (5 weeks), *n* = 12 (14 weeks), and *n* = 10 (23 weeks). Scale bar: 1 mm.
- G Higher magnification of PAS- and Picosirius Red (lower right)-stained sections showing dilated tubules (upper left), thickened tubular basement membranes (arrowheads, upper right), interstitial inflammation (lower left), and interstitial fibrosis (lower right) in 23-week-old *Lkb1*^{ATub} mice. Scale bar: 50 μ m. See also Fig EV1L.
- H Transmission electron microscopy of distal tubule from 14-week-old *Lkb1*^{ATub} mice. Dotted lines indicate thickening of basement membrane (lower panel). Representative images of *n* = 3 mice. Scale bars: 2 μ m.

Data information: In (D, E), filled circles: control mice; and open circles: *Lkb1*^{ATub} mice. Each circle represents one individual mouse. In (D), bars indicate mean. Mann–Whitney, ***P* < 0.01, ****P* < 0.001.

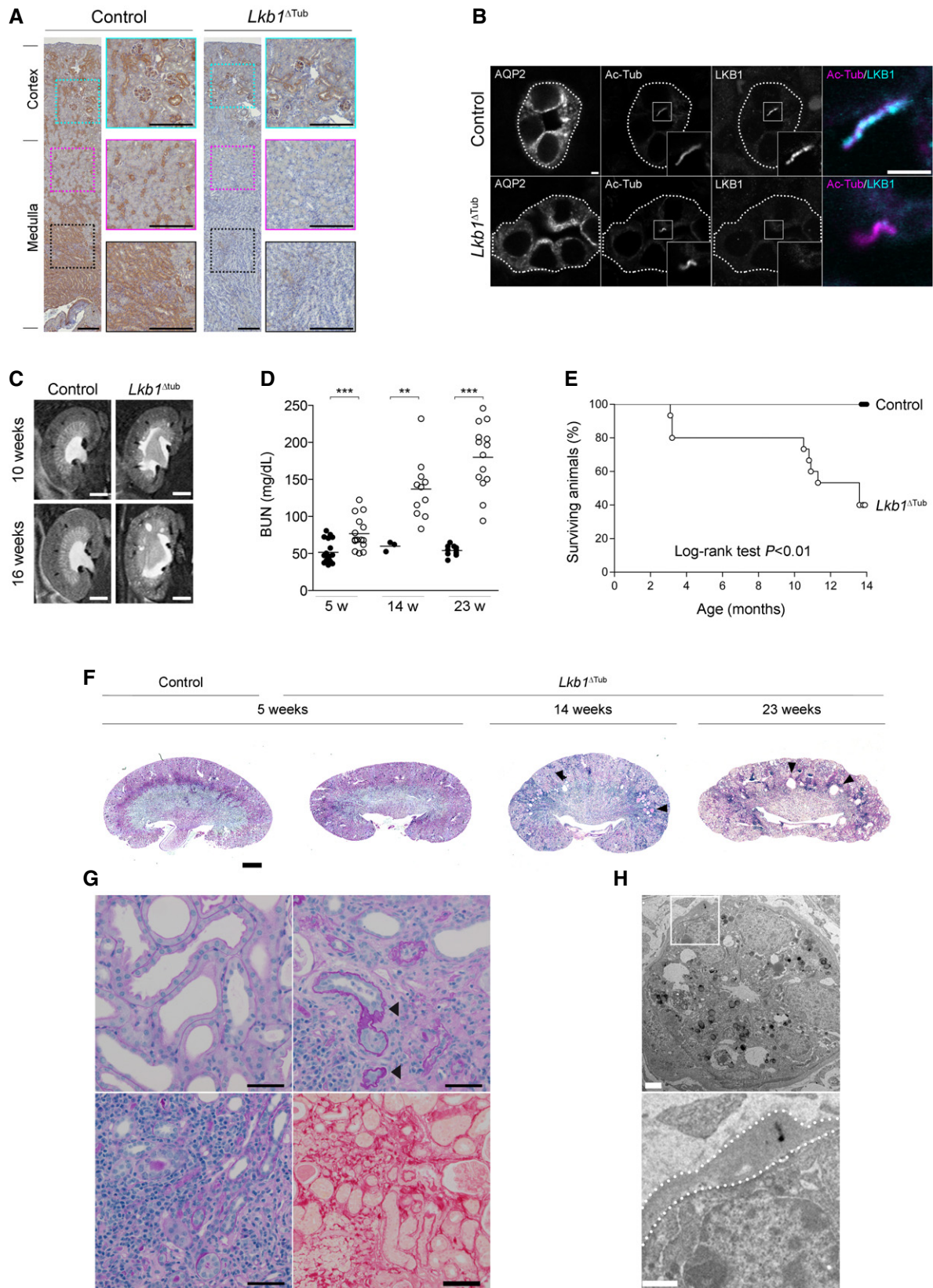


Figure 1.

junction (Fig 1C and F; 14 and 23 weeks). Histology revealed dilated tubules, thickened tubular basement membranes, interstitial inflammation, and fibrosis (Fig 1G and H). These findings are similar to those of a previous study, which investigated renal metabolism using the same mouse genotype that was created independently (Han *et al*, 2016).[#] Collagen synthesis, a marker for extracellular matrix deposition, was increased (Fig EV1L), and renal failure ensued (Fig 1D and E). Analogous to humans with Peutz-Jeghers syndrome, heterozygote animals had normal renal function and histology (Appendix Fig S1). These findings show that LKB1 is required for normal morphology and function of the kidney. Loss of LKB1 in the kidney results in alterations of tubular architecture, cysts, and chronic inflammation with progressive scarring leading to renal failure, reminiscent of a renal ciliopathy phenotype.

LKB1 interacts with ciliopathy proteins, and a functional interaction exists between LKB1 and NPHP1

To obtain insights into what might explain the phenotype of LKB1 deletion in the kidney, we performed a proteomic screen in protein lysates from renal medulla, aiming to identify endogenous interactors of LKB1 that might illuminate its function. The LKB1 precipitates obtained from these lysates were highly enriched for the known LKB1 interactor STRADa and 30 other proteins (Fig 2A and Datasets EV1 and EV2). Of these, 12 have previously been implicated in renal physiology or development (Dataset EV1). Two of them have been linked to the renal ciliopathy nephronophthisis (NPHP): ANKS3 (ankyrin repeat and sterile alpha motif domain containing 3) and NEK7 (NIMA (never in mitosis gene A)-related kinase 7). ANKS3 is a ciliopathy protein and a known interactor of several proteins involved in NPHP, including NPHP1 (Leetola *et al*, 2014; Yakulov *et al*, 2015; Shamseldin *et al*, 2016), the protein mutated in 60% of patients with genetically defined NPHP (Hildebrandt *et al*, 1997; Saunier *et al*, 1997; Halbritter *et al*, 2013; König *et al*, 2017). ANKS3 also has a physical and functional interaction with NEK7, and NEK7 is part of the cilia proteome (Mick *et al*, 2015; Ramachandran *et al*, 2015). We confirmed the endogenous interaction between LKB1, ANKS3, and NEK7 by co-immunoprecipitations from

renal medulla (Fig 2B) and found that ANKS3 localizes to cilia (Fig 2C–E and Appendix Fig S3F).

The interaction between LKB1 and two cilia proteins associated with NPHP1 is interesting, since the phenotype of the *Lkb1*^{ΔTub} mice resembles NPHP in children. Furthermore, it suggests a functional synergy between LKB1 and NPHP1. Indeed, LKB1 co-immunoprecipitated with NPHP1 (Figs 2F and EV2A), but interacted only weakly with NPHP2, NPHP3, NPHP4, and NPHP8 (Fig EV2B and C). To test whether LKB1 and NPHP1 have a functional interaction, we used zebrafish, an established model for ciliopathy phenotypes (Kramer-Zucker *et al*, 2005; Tuz *et al*, 2014). Morpholino-mediated knockdown of NPHP proteins and *anks3* in zebrafish larvae results in the formation of pronephric cysts (Yakulov *et al*, 2015). We found that knockdown of *nphp1* caused cyst formation in a minority of larvae, whereas knockdown of *lkb1* alone had no effect (Fig 2G and H). However, co-injection of both morpholinos strongly increased the proportion of larvae with a cystic phenotype (Fig 2H). Taken together, these findings link LKB1 and NPHP1 in physical and functional terms. They suggest that LKB1 is in a complex with NPHP1, ANKS3, and NEK7, and open the possibility that this module regulates signaling events downstream of cilia relevant to the observed renal phenotype.

Loss of LKB1 results in epithelial upregulation of CCL2 and is associated with the accumulation of CCR2⁺ macrophages

We were interested in the downstream events explaining the inflammation and fibrosis in *Lkb1*^{ΔTub} kidneys. The best characterized target of LKB1 signaling is the AMP sensing kinase AMPK, but other downstream substrates are known (Lizcano *et al*, 2004; Shaw *et al*, 2004). LKB1 phosphorylates AMPK to inhibit mTORC1 and protein synthesis. We did not find consistent signals demonstrating dysregulation of AMPK or mTORC1 signaling in the tubules of *Lkb1*^{ΔTub} kidneys (Appendix Fig S2), suggesting that alternative signaling events triggered by LKB1 inactivation are involved in the renal pathology. To approach this issue in an unbiased fashion, we performed microarray analysis in *Lkb1* mutant kidneys at an early time point, when there was only little damage to the parenchyma (Fig 1F; 5 weeks). We compared these data with RNAseq analyses

Figure 2. LKB1 interacts with ANKS3, NEK7, and NPHP1.

- A LKB1 interactors identified by a proteomic screen in mouse kidney medulla. See also Datasets EV1 and EV2.
 B Immunoprecipitates (IP) from mouse kidney medulla. ANKS3 and NEK7 are enriched in the LKB1 precipitates. Representative Western blot of three independent experiments. Expected molecular weights: ANKS3 (72 kDa), LKB1 (54 kDa), and NEK7 (35 kDa).
 C Representative confocal microscopy images of primary cilia (acetylated tubulin expressing, Ac-Tub) and ANKS3 in MDCK cells expressing inducible shRNA against Anks3 (*Anks3-i1*) after tetracycline induction (Tet). Scale bar: 5 μm. See also Appendix Fig S3F.
 D Quantification of ANKS3-positive primary cilia in *Anks3-i1* MDCK cells. Blinded quantification of five fields of view per biological replicate.
 E Confocal microscopy images of collecting duct (AQP2 expressing) from 5-week-old wild-type mice. Anti-ANKS3 antibody (upper panel), but not control IgG (lower panel), detects a signal in cilia (Ac-Tub). Representative images of *n* = 5 mice. Scale bar: 5 μm.
 F IP from HEK 293T cells. Endogenous LKB1 is enriched in the precipitates of FLAG-NPHP1. Representative Western blot of three independent experiments. See also Fig EV2A–C.
 G Zebrafish embryos injected with control morpholino (MO) or MO targeting *nphp1* at 48 h post-fertilization. Arrowheads indicate pronephric cysts. Scale bar: 100 μm.
 H Quantification of embryos with pronephric cysts. Numbers in bars represent *n* analyzed embryos.
 Data information: In (D), each circle represents one biological replicate. Bars indicate mean. Paired *t*-test, **P* < 0.05. In (H) mean ± SD. ANOVA followed by the Tukey–Kramer test, **P* < 0.05, ***P* < 0.01.
 Source data are available online for this figure.

[#]Correction added on 1 August 2018 after first online publication: This sentence and new reference Han *et al* (2016) were added.

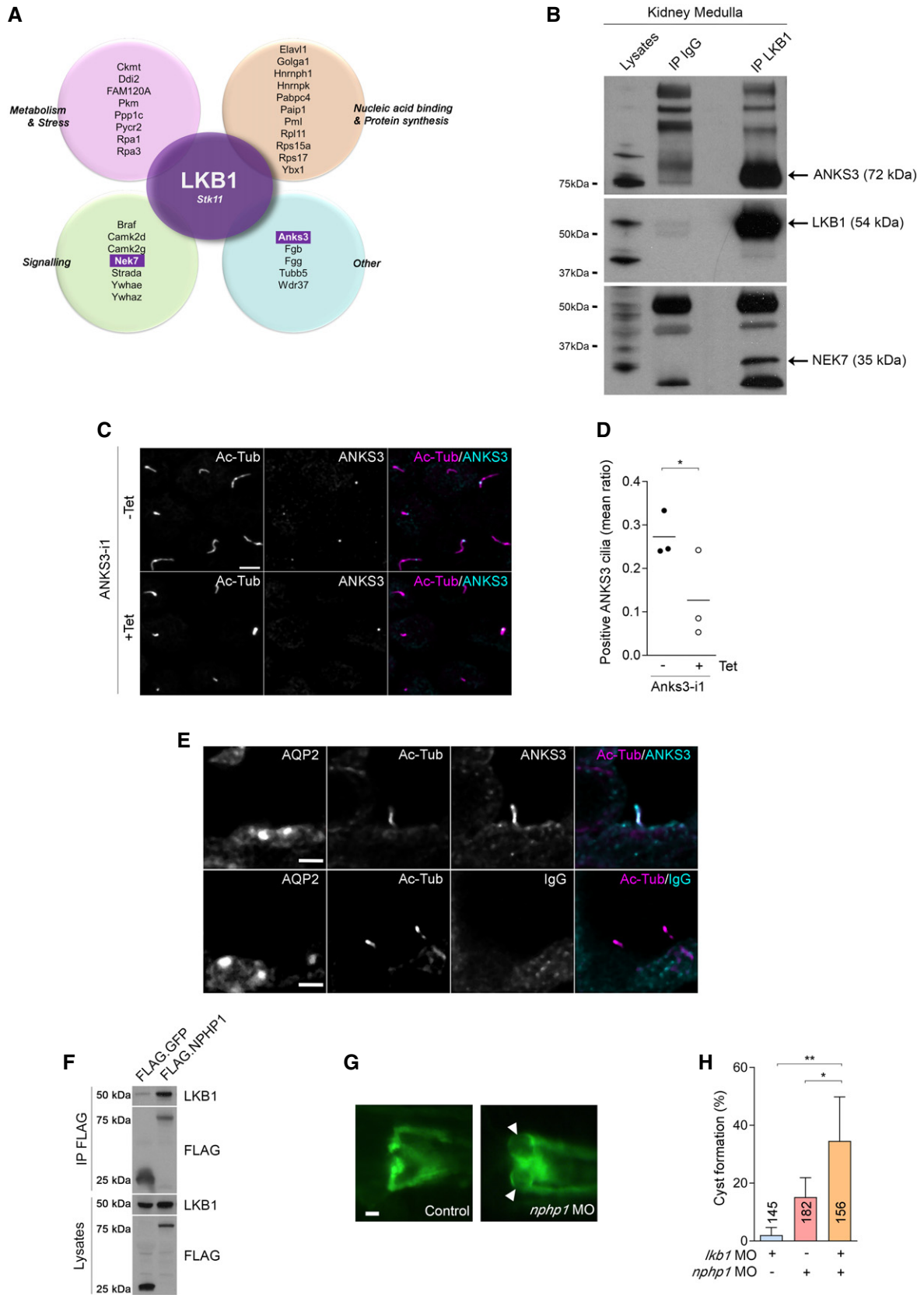


Figure 2.

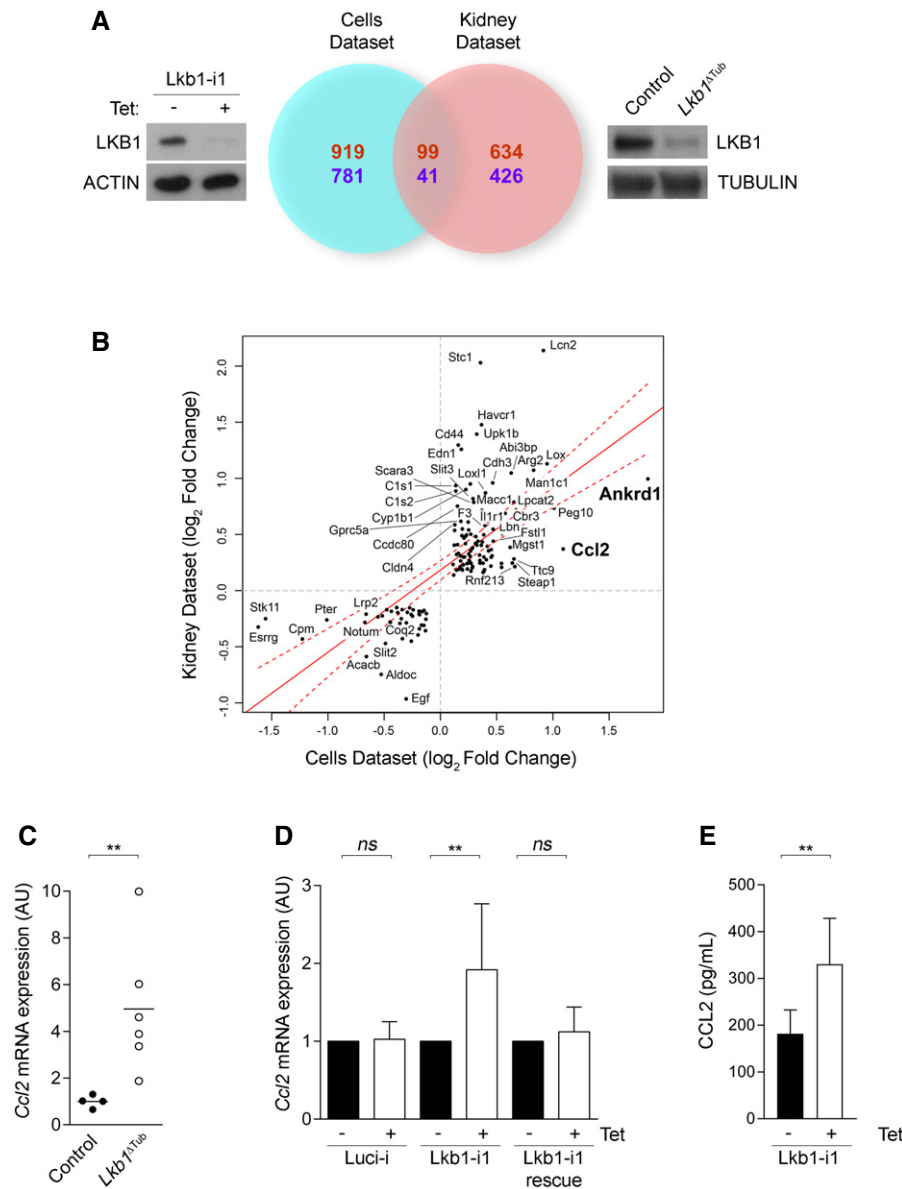


Figure 3. Transcriptome analysis in LKB1-deficient kidneys and a renal epithelial cell line depleted of LKB1.

A Venn diagram of differentially regulated genes from *Lkb1*-depleted MDCK cells (left *Lkb1*-i1 + tetracycline) and kidneys from *Lkb1^{ΔTub}* mice (right). Red numbers: upregulated; blue numbers: downregulated. See also Fig EV3A–C and Datasets EV3–EV5.
B Jointly up- and downregulated genes in the mouse (kidney dataset) and MDCK cells (cells dataset) (FDR < 0.05, Pearson correlation $r = 0.69$). Genes with a combined fold change > 0.6 are annotated. *Ccl2* and *Ankrd1* are referred to in the text. Solid line: linear fit; dotted lines: 95% confidence interval.
C *Ccl2* mRNA expression in kidney medulla from littermate control and *Lkb1^{ΔTub}* mice at 5 weeks.
D *Ccl2* mRNA expression in MDCK cells expressing inducible shRNA against the indicated targets after tetracycline treatment (Tet). Luci-i (shRNA against luciferase; $n = 7$), *Lkb1*-i1 ($n = 8$), and *Lkb1*-i1 rescue ($n = 5$). See also Fig EV3D and Appendix Fig S3A–C.
E CCL2 secretion in *Lkb1*-i1 MDCK cell supernatants after tetracycline induction (Tet). ($n = 5$).

Data information: In (C), each circle represents one individual mouse. Bars indicate mean. Mann–Whitney, $**P < 0.01$. In (D, E) mean \pm SD. Paired t-test, $**P < 0.01$, ns: not statistically different.

Source data are available online for this figure.

performed in MDCK cells where *Lkb1* was depleted by shRNA-induced knockdown (Boehlke et al, 2010b; Figs 3A and EV3A and B, and Dataset EV3). This approach allowed us to discard regulated transcripts from the kidney that came from outside renal epithelia. At the same time, it enabled us to look at transcripts that we might

have discarded, if we had assumed that they originate in non-epithelial cells, for instance immune cells. Network analysis of clustered GO terms for the 99 commonly upregulated genes revealed changes in biological processes relating to organ development, morphogenesis, and angiogenesis which are in keeping with the role of LKB1 in

early development and cancer (Fig EV3C and Dataset EV4), while the 41 downregulated genes represented mostly metabolic processes (Dataset EV5). Surprisingly, the upregulated genes revealed clusters incorporating immune response, cytokine production, and immune cell migration (Fig EV3C). The two most highly upregulated genes in the renal tubular cell-derived set that were co-regulated *in vivo* were the cytokine-inducible transcription factor ANKRD1 (ankyrin repeat domain 1) and the inducible cytokine CCL2 (chemokine (C-C motif) ligand 2; Fig 3B and Dataset EV3).

CCL2 (also known as monocyte chemoattractant protein 1 or MCP1) is a potent chemoattractant of bone marrow-derived CCR2⁺ blood monocytes which are critical progenitors for tissue macrophages in many pathological conditions, including bacterial immunity, tumors, and inflammation (Serbina & Pamer, 2006; Franklin et al, 2014; Cao et al, 2015). As CCL2 has been shown to promote macrophage recruitment and disease progression in chronic kidney disease (Cao et al, 2015), we focused our attention on this protein. CCL2 upregulation was confirmed in *Lkb1* mutant kidneys as well as in cells after shRNA-mediated depletion of LKB1 and was prevented by AICAR treatment (Figs 3C–E and EV3D and E, and Appendix Fig S3). These data identify CCL2 as a highly upregulated chemokine in the kidney after loss of LKB1 *in vivo*. Our *in vitro* data demonstrate that renal tubular cells are the source of CCL2 in LKB1 deficiency.

To better characterize the local inflammatory response triggered by inactivation of *Lkb1 in vivo*, we analyzed renal cell suspensions from *Lkb1* mutant mice and littermate controls by flow cytometry (Triantafyllou et al, 2010; Appendix Fig S5): *Lkb1* mutant mice contained significantly increased numbers of CD45-positive leukocytes. This was in part explained by increased numbers of neutrophils, while B- and T-cell numbers were not significantly changed. Strikingly, kidney monocytes and CD11b^{hi} macrophages expressing CCR2, the CCL2 receptor, were significantly increased (Fig 4A–F and Appendix Fig S5). These findings support the notion that LKB1-deficient renal epithelial cells in the kidney take on an inflammatory phenotype and release CCL2, resulting in the recruitment of mononuclear phagocytes and macrophage activation.

The LKB1/NPHP1/ANKS3/NEK7 complex controls CCL2 expression

The data described above raise two questions: (i) Does the complex of LKB1 with NPHP1, ANKS3, and NEK7 regulate CCL2? (ii) If so, does this regulation require cilia? To address the first question, we resorted to a loss-of-function approach using shRNA-mediated knockdown in cultured renal epithelial cells. Remarkably, depletion of NPHP1 but not NPHP4 resulted in upregulation of *Ccl2* in MDCK cells (Fig 5A and Appendix Fig S3). Similar to the findings in NPHP1 or LKB1 knockdown cells, *Ccl2* was increased in cells depleted of

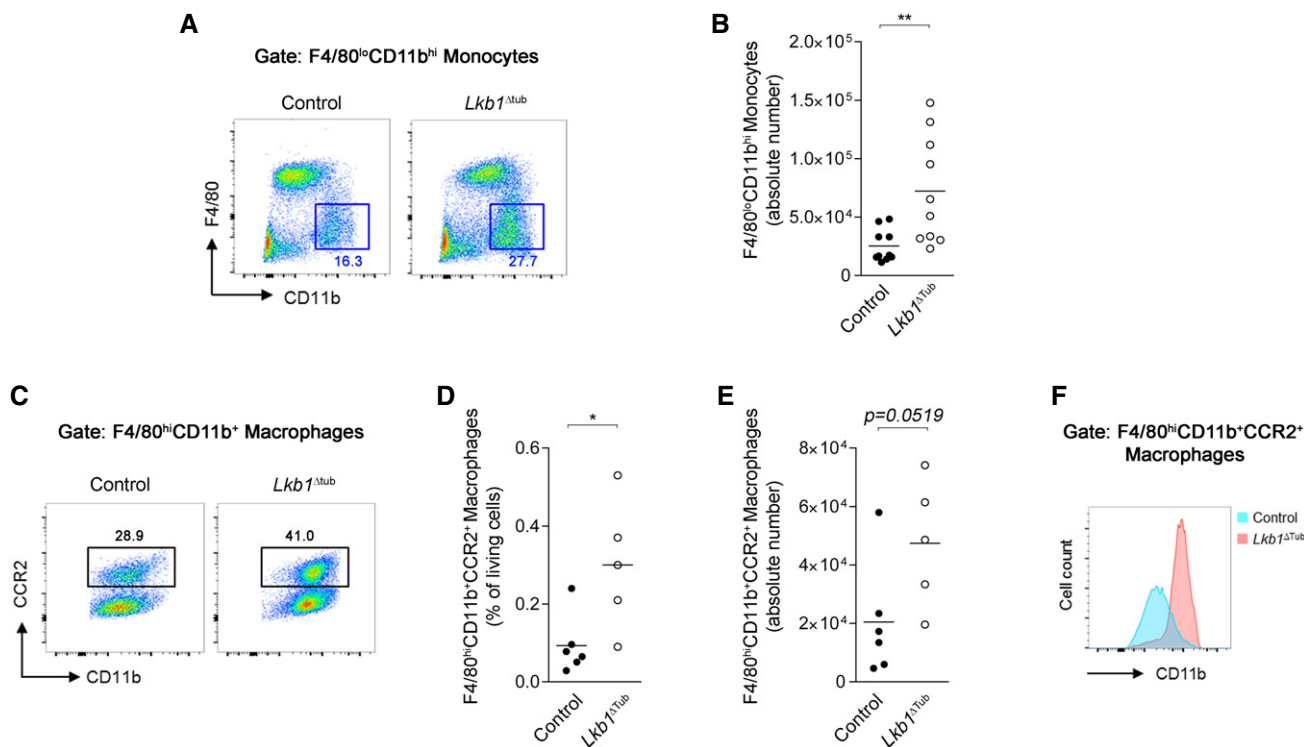


Figure 4. Monocytes and CCR2⁺ macrophage accumulation in the kidneys of *Lkb1*^{ΔTub} mice.

A, B Flow cytometry analysis (A) and absolute numbers (B) of kidney monocytes (F4/80^{lo}CD11b^{hi}, blue rectangles) at 10 weeks. See also Appendix Fig S5.

C–E Flow cytometry analysis (C), percentage (D), and absolute numbers (E) of CCR2⁺ macrophages (F4/80^{hi}CD11b⁺CCR2⁺, black rectangles) at 10 weeks.

F Flow cytometry analysis of CD11b expression in F4/80^{hi}CD11b⁺CCR2⁺ macrophages at 10 weeks.

Data information: In (A, C), numbers below or above rectangles represent percentage of cells per area. In (B–E), each circle represents one individual mouse. Bars indicate mean. Mann–Whitney, **P* < 0.05, ***P* < 0.01.

ANKS3 or NEK7, while total LKB1 expression was not affected (Figs 5B and EV3F and G, and Appendix Figs S3 and S4). This indicates that LKB1, NPHP1, ANKS3, and NEK7 act as signaling modules to suppress this chemokine.

The ciliary isoform of the LKB1 interactor STRAD is required for CCL2 regulation

Liver kinase B1, in addition to the cilium, resides in the nucleus and the cytosol. To clarify whether the LKB1 module acts in cilia, we sought evidence that ciliary localization of LKB1 is required for suppression of CCL2. To address this question, we focused on the functional LKB1 interactors STRADa and STRADb (Zequiraj *et al*, 2009) which are part of a heterotrimeric complex and required for the kinase activity of LKB1 (Baas *et al*, 2003; Boudeau *et al*, 2003). Indeed, we found that NPHP1 interacts with STRAD, supporting a functional role of the LKB1–NPHP1 interaction (Fig EV2D). STRADb has been reported to mediate entry of LKB1 into cilia, whereas STRADa is required for LKB1 function in the cytosol (Boudeau *et al*, 2003; Mick *et al*, 2015). Indeed, we found that tagged versions of STRADb, but not STRADa, localized to cilia in MDCK cells (Fig 5C). Furthermore, inducible knockdown of STRADb decreased the amount of LKB1 in the cilium (Fig 5D and E and Appendix Fig S3). Notably, depletion of STRADb recapitulated the *Ccl2* increase seen after LKB1 or NPHP1 depletion, whereas this was not the case for knockdown of STRADa (Fig 5F and Appendix Fig S3). Since STRADb is the functional interactor of LKB1 within the cilium, these data confirm that LKB1 is required within cilia to regulate CCL2.

Primary cilia are positive regulators of CCL2

At this point, our findings suggested two possible alternatives of how cilia might regulate CCL2. They could act either as negative regulators of CCL2, in which case removal of cilia would increase expression of CCL2, or as sensors of a CCL2-inducing signal that is negatively regulated by the LKB1 module, in which case removal of the cilium would decrease CCL2 levels. A similar mechanism has been described for hedgehog, a developmental pathway that processes crucial signaling steps within cilia (Corbit *et al*, 2005; Bangs & Anderson, 2017). Indeed, we found the second possibility to be the case. We ablated cilia by interfering with intraflagellar transport (IFT). Targeting the ciliary kinesin subunit KIF3a or the IFT protein IFT88 prevents cells from forming cilia (Marszalek *et al*, 1999; Pazour *et al*, 2000; Boehlke *et al*, 2010b). We found that

cilia-deficient compared to ciliated cells expressed lower levels of *Ccl2* (Fig 5G and Appendix Fig S3). Furthermore, co-ablation of cilia together with LKB1 prevented the increase in *Ccl2* that is seen after LKB1 depletion alone (Fig 5H and Appendix Fig S3), suggesting that cilia are required for the upregulation of CCL2 and that the LKB1 module inhibits cilia-induced CCL2 expression (Fig 8A and B).

PKD1 interacts with LKB1 and STRAD

A cilia-dependent cyst-activating mechanism has been postulated for the ciliopathy ADPKD (Ma *et al*, 2013). This mechanism is inhibited by PKD1 under physiological conditions and is released in the presence of a PKD mutation, driving cyst growth. However, the putative ciliary downstream signal has not been identified. We therefore wondered whether deregulated CCL2 control by dysfunction of the LKB1 module in cilia plays a role in ADPKD. Consistent with this notion, we found that PKD1 co-immunoprecipitates with LKB1 and both STRADa and STRADb (Fig 6A). Furthermore, analyzing PKD1-null renal epithelial cells that were constructed using TALEN-based genome editing (Appendix Fig S3; Hofherr *et al*, 2017), we observed that *Ccl2* was upregulated compared to wild-type cells (Fig 6B and C), analogous to our findings in LKB1-depleted cells. Neither LKB1 nor other members of the regulatory complex were consistently altered in their expression (Appendix Fig S4). When we ablated cilia through depletion of KIF3a or IFT88 in *Pkd1*-null cells, we found a marked decrease in *Ccl2* (Fig 6D and Appendix Fig S3). Simultaneous LKB1 depletion in PKD1 knockout cells, however, did not change *Ccl2* expression compared to PKD1 deletion alone (Fig EV3H and Appendix Fig S3), indicating that PKD1 is required for LKB1 to repress *Ccl2* expression. Taken together, these findings, obtained *in vitro* in a cell-based system, demonstrate that a physical and functional interaction exists between PKD1 and the LKB1 module. Our findings suggest that PKD1 and the LKB1 module form a functional unit to inhibit a ciliary CCL2-inducing signal and that PKD1 is required for its function. This raised the possibility that deregulation of CCL2 may play a role in the pathological changes occurring in ADPKD.

Cilia-induced CCL2 promotes disease progression in a mouse model of ADPKD

Inflammation and fibrosis lead to a loss of parenchyma and small kidneys in patients with NPHP (Konig *et al*, 2017). In ADPKD, however, macrophages have been shown to be activators of cyst

Figure 5. LKB1 acts in concert with NPHP1, ANKS3, and NEK7 to regulate CCL2 in a cilium-dependent manner.

- A, B *Ccl2* mRNA expression in MDCK cells expressing inducible shRNA against the indicated targets (+ Tet). *Nphp1-i* ($n = 8$), *Nphp4-i* ($n = 4$), *Anks3-i1* ($n = 5$), and *Nek7-i1* ($n = 5$). See also Appendix Fig S3D–G.
- C Confocal microscopy images of primary cilia (Ac-Tub) and GFP in MDCK wild-type cells (WT) or in MDCK cells expressing GFP alone or YFP constructs fused to LKB1 or STRAD proteins. GFP antibody was used to detect both GFP and YFP constructs. Representative images of three biological replicates. Scale bar: 1 μm .
- D Representative confocal microscopy images of primary cilia (Ac-Tub) and LKB1 in MDCK cells expressing inducible shRNA against *Stradb* (*Stradb-i*; + Tet). Scale bar: 5 μm (left panel) and 1 μm (right panel). See also Appendix Fig S3I.
- E Quantification of LKB1-positive primary cilia in *Stradb-i* MDCK cells. Blinded quantification of five fields of view per biological replicate.
- F *Ccl2* mRNA expression in *Strada-i* ($n = 5$) and *Stradb-i* ($n = 5$) MDCK cells. See also Appendix Fig S3H and I.
- G, H *Ccl2* mRNA expression in MDCK cells expressing inducible shRNA against the indicated targets (+ Tet). *Kif3a-i* ($n = 7$), *Ift88-i* ($n = 4$), *Kif3a-i*; *Lkb1-i1* ($n = 3$), and *Ift88-i*; *Lkb1-i1* ($n = 4$). See also Appendix Fig S3J–M.

Data information: In (A, B, F–H), mean \pm SD. Paired *t*-test, * $P < 0.05$, ** $P < 0.01$, *** $P < 0.001$, ns: not statistically different. In (E), each circle represents one biological replicate. Bars indicate mean. Paired *t*-test, * $P < 0.05$.

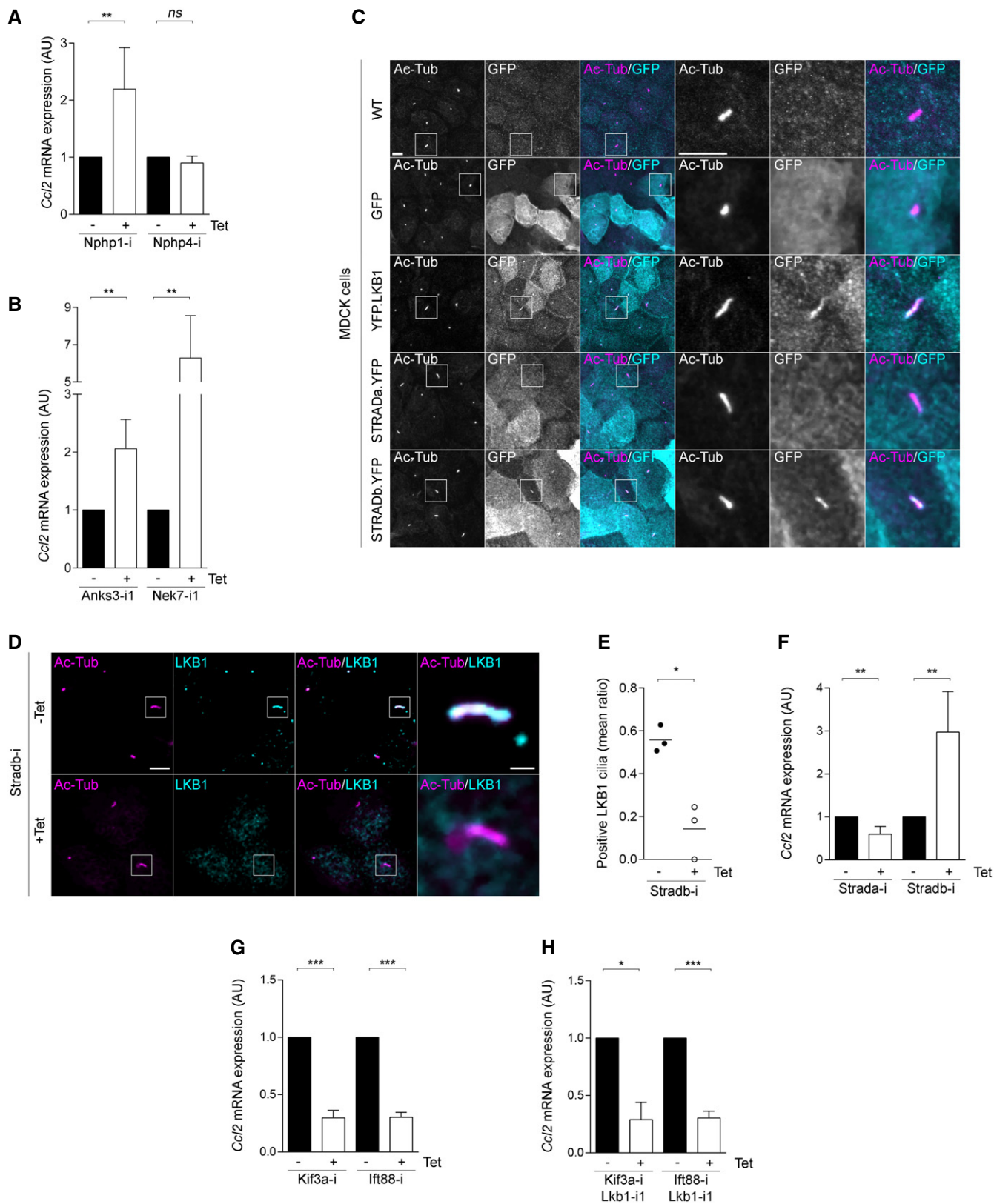


Figure 5.

growth, thus leading to kidney enlargement and disease progression (Karihaloo *et al*, 2011), providing a rationale for the hypothesis that the regulatory effect of PKD1 and LKB1 on cilia-induced CCL2 expression is relevant for human pathology. We tested this hypothesis in an orthologous model of ADPKD, where post-natal inactivation of *Pkd1* results in slow-onset PKD, recapitulating human disease (Ma *et al*, 2013; Figs 6E and F, and EV4). In these kidneys, we observed that an early stage of cyst formation was accompanied by the upregulation of *Ccl2* transcript but no change in LKB1 or other members of the regulatory complex (Fig 6G and Appendix Fig S4). Flow cytometry analysis revealed that CCR2⁺ kidney mononuclear phagocytes were markedly increased in *Pkd1*-deficient kidneys (Fig 6H–K). In contrast, kidney B and T lymphocytes and neutrophils were not significantly increased at this early time point (Appendix Fig S6).

To test whether cilia are required for the upregulation of CCL2 in *Pkd1*-deficient kidneys, we generated mice with simultaneous targeting of *Pkd1* and *Kif3a*. As has been described (Ma *et al*, 2013), these animals had a strongly ameliorated phenotype (Figs 6E and F, and EV4). In line with our *in vitro* findings, disruption of ciliogenesis prevented *Ccl2* upregulation in *Pkd1*-deficient kidneys (Fig 6G). Concurrently, cilia ablation also decreased the numbers of CCR2⁺ mononuclear phagocytes (Fig 6H–K).

This finding supports the hypothesis that cilia induce CCL2 in *Pkd1*-deficient kidneys to recruit macrophages and drive cyst growth. However, it leaves the possibility that an unknown ciliary signal other than CCL2 drives cyst growth, affecting inflammation and immune cell-mediated CCL2 expression by indirect means. To investigate this possibility, we inactivated *Pkd1* and *Ccl2* simultaneously in renal epithelial cells using the same Cre driver. As expected, this resulted in fewer macrophages and a strongly ameliorated phenotype (Figs 7A–E and EV5). This finding confirms that tubular CCL2 drives ADPKD severity *in vivo*.

Our findings from *in vitro* systems and an ADPKD model demonstrate that PKD1 interacts with the LKB1 regulatory module to inhibit a ciliary signal inducing CCL2 (Fig 8C). A *Pkd1* mutation releases the inhibitory signal, promoting increased levels of CCL2, the accumulation of CCR2⁺ mononuclear phagocytes, and cyst growth, while the ablation of cilia or inactivation of CCL2 in PKD1 mutant epithelial cells in the kidney prevents this cascade (Fig 8D–F).

Discussion

We define here that cilia of renal tubules actively regulate peritubular macrophage numbers. Cilia act as signal transducers to increase expression of the chemokine CCL2. The signal inducing CCL2 is regulated by a ciliary module involving LKB1, the ciliopathy proteins NPHP1, PKD1, and ANKS3, and NEK7. Genetic targeting of *Lkb1* or *Pkd1* in the kidney *in vivo* results in mononuclear phagocyte recruitment and the promotion of ciliopathy phenotypes. Ablation of cilia or CCL2 in *Pkd1* mutant mice prevents this pathophysiology and ameliorates the disease.

The loss of LKB1 in kidney tubules leads to a progressive disruption of renal architecture and function resembling a nephronophthisis phenotype. These events are characterized by inflammation and fibrosis and involve the secretion of CCL2 and expansion of CCR2⁺ macrophages. LKB1 regulates CCL2 by interacting with three proteins linked to NPHP, a ciliopathy occurring in children and adolescents. Among them is NPHP1, the protein most commonly mutated in genetically defined NPHP, and two interacting cilia proteins: ANKS3 and NEK7, the first of which is a ciliopathy protein itself. All of these proteins are required for CCL2 regulation.

The LKB1 regulatory module acts within cilia: LKB1 exerts its CCL2-suppressive function only in the presence of the cilia-specific LKB1 interactor STRADb, but not in its absence when only the cytosolic STRADa is present. In the absence of cilia, CCL2 does not increase, suggesting that cilia carry a positive signal regulating CCL2 which is blocked by the LKB1 module. This is supported *in vivo* by the finding that ablation of cilia or CCL2 together with PKD1 ameliorates the cystic phenotype in a similar manner.

Our findings suggest that this mechanism is relevant for the human ciliopathy ADPKD. Based on observations in orthologous mouse models that ablation of cilia ameliorates the ADPKD phenotype, it has been proposed that PKD1 blocks a cilia-dependent cyst-activating signal whose nature has not been specified (Ma *et al*, 2013). Indeed, CCL2 is such a signal: We find that PKD1 interacts with LKB1 and its functional interactor STRAD. Loss of PKD1 *in vitro* and *in vivo* stimulates CCL2 expression in a cilia-dependent way: In a PKD1 mouse model, we find that lack of cilia results in lower amounts of CCR2⁺ macrophages and decreased cyst

Figure 6. PKD1 interacts with LKB1 to prevent the cilium-dependent CCL2 increase and inflammation.

- A Immunoprecipitation (IP) from HEK 293T cells. FLAG-PC1 is enriched in the precipitates of V5-LKB1, V5-STRADa, and V5-STRADb. Representative Western blot of five independent experiments.
- B *Ccl2* mRNA expression in wild-type (WT) and two PKD1-null (KO1, KO2) MDCK cell lines constructed using TALEN-based genome editing ($n = 4$). See also Appendix Fig S3N–P.
- C CCL2 secretion in WT and PKD1 KO1 and KO2 MDCK cell lines ($n = 3$).
- D *Ccl2* mRNA expression in PKD1 KO1 MDCK cells expressing inducible shRNA against the indicated targets after tetracycline induction (Tet). WT ($n = 4$), *Kif3a*-i ($n = 4$), and *Ift88*-i ($n = 4$). See also Appendix Fig S3Q and R.
- E Representative kidneys from control, *iPkd1*^{ΔTub}, and *iPkd1*^{ΔTub};*iKif3a*^{ΔTub} mice at 12 weeks. See also Fig EV4.
- F Kidney weight (KW)-to-body weight (BW) ratio in control, *iPkd1*^{ΔTub}, and *iPkd1*^{ΔTub};*iKif3a*^{ΔTub} mice at 12 weeks.
- G *Ccl2* mRNA expression in kidneys from control, *iPkd1*^{ΔTub}, and *iPkd1*^{ΔTub};*iKif3a*^{ΔTub} mice at 12 weeks.
- H, I Flow cytometry analysis (H) and absolute numbers (I) of CCR2⁺ macrophages (F4/80^{hi}CD11b⁺CCR2⁺, black oval) in control, *iPkd1*^{ΔTub}, and *iPkd1*^{ΔTub};*iKif3a*^{ΔTub} mice at 12 weeks. See also Appendix Fig S6.
- J, K Flow cytometry analysis (J) and absolute numbers (K) of CCR2⁺ monocytes (F4/80^{lo}CD11b^{hi}CCR2⁺, black square) in control, *iPkd1*^{ΔTub}, and *iPkd1*^{ΔTub};*iKif3a*^{ΔTub} mice at 12 weeks.

Data information: In (B–D), mean ± SD. Paired t-test, * $P < 0.05$. In (F, G, I, K), each dot represents one individual mouse. Bars indicate mean. ANOVA followed by the Tukey–Kramer test, * $P < 0.05$, *** $P < 0.001$. In (H, J), numbers represent percentage of cells per gated region.

Source data are available online for this figure.

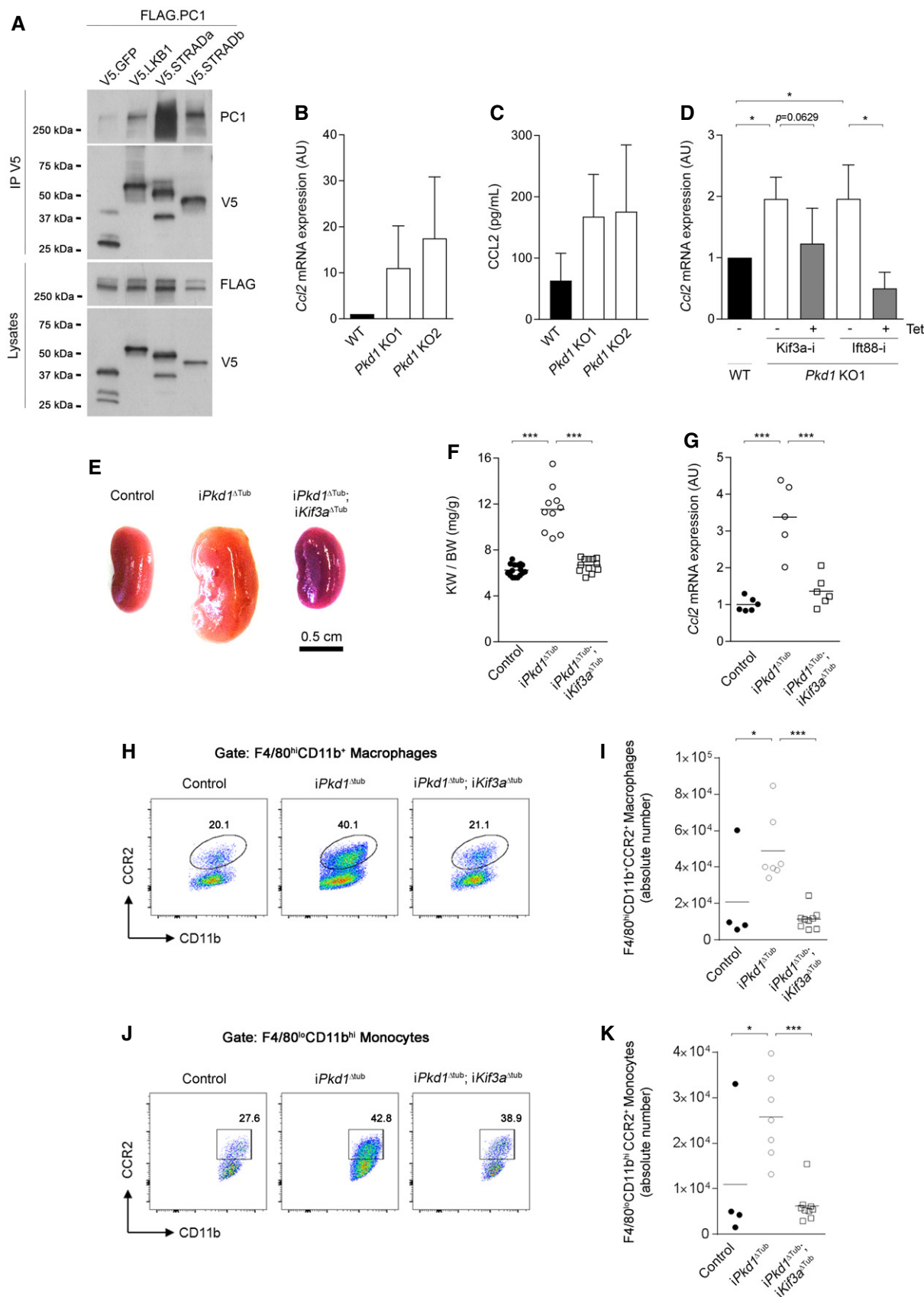


Figure 6.

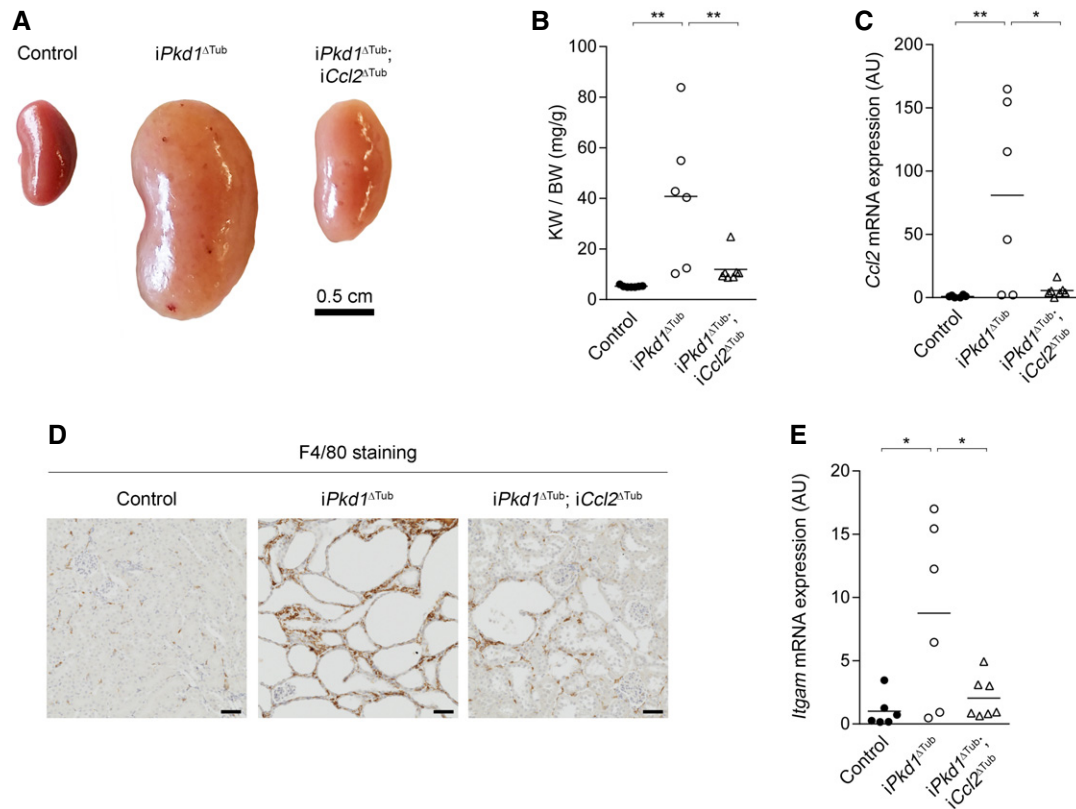


Figure 7. Tubule-derived CCL2 promotes macrophage recruitment and cyst formation in *Pkd1*-targeted kidneys.

A Representative kidneys from control, *iPkd1*^{ΔTub}, and *iPkd1*^{ΔTub}; *iCcl2*^{ΔTub} mice at 13.5 weeks. See also Fig EV5.
 B Kidney weight (KW)-to-body weight (BW) ratio in control, *iPkd1*^{ΔTub}, and *iPkd1*^{ΔTub}; *iCcl2*^{ΔTub} mice at 13.5 weeks.
 C *Ccl2* mRNA expression in kidneys from control, *iPkd1*^{ΔTub}, and *iPkd1*^{ΔTub}; *iCcl2*^{ΔTub} mice at 13.5 weeks.
 D F4/80 immunostaining in kidneys from control, *iPkd1*^{ΔTub}, and *iPkd1*^{ΔTub}; *iCcl2*^{ΔTub} mice at 13.5 weeks. Representative images of *n* = 4 mice/group. Scale bars: 50 μm.
 E *Itgam* mRNA expression in kidneys from control, *iPkd1*^{ΔTub}, and *iPkd1*^{ΔTub}; *iCcl2*^{ΔTub} mice at 13.5 weeks.

Data information: In (B, C, E), each dot represents one individual mouse. Bars indicate mean. ANOVA followed by the Tukey–Kramer test, **P* < 0.05, ***P* < 0.01.

formation. In addition, deletion of CCL2 concomitant with PKD1 in renal tubules reduces macrophage numbers and ameliorates cyst formation. These findings are consistent with previously published data showing that macrophage recruitment is a driving force for cyst growth in different animal models of PKD (Cowley *et al*, 2001; Karihaloo *et al*, 2011; Norman, 2011; Chen *et al*, 2015; Puri *et al*, 2016). Indeed, in human patients CCL2 excretion in the urine has been found to be a marker of ADPKD progression (Zheng *et al*, 2003), suggesting that the regulation of CCL2 by the ciliary LKB1 module is clinically important.

Could there also be a wider role for ciliary LKB1 in renal disease? Inflammation and fibrosis represent a final common pathway in different types of chronic renal disease (Cao *et al*, 2015), but in a large number of cases, the inflammatory trigger is not established. In the German chronic kidney disease cohort, with over 5,000 participants, less than one-third of the patients had an underlying chronic inflammatory disorder such as autoimmune disease (Titze *et al*, 2015). Among the remaining patients, the causes were diabetes (15%), vascular (25%), or undetermined (21%). Both diabetes and vascular disease are metabolic disorders. Of note, LKB1 is a metabolic sensor and CCL2 signaling has been implicated in diabetic kidneys and vascular disease (Sayyed *et al*, 2011; Bot *et al*, 2017).

This raises the possibility that in metabolic disease, the ciliary LKB1 module could confer an inflammatory phenotype on renal epithelial cells to mediate chronic inflammation in the kidney. Given that chronic kidney disease is now the tenth leading cause of death worldwide (Eckardt *et al*, 2013; GBD2015-Collaborators, 2016), this is of considerable interest.

Liver kinase B1 might link cilia to inflammation also outside the kidney: Obesity and diabetes are states of energy excess, and metformin, an antidiabetic drug that augments the effect of LKB1 on AMPK, is particularly effective in obese diabetics (UKPDS Group, 1998). Obesity and diabetes are accompanied by low-grade inflammation in a positive feedback loop, particularly in adipose tissue, where adipocytes release CCL2 to recruit CCR2-expressing monocytes (Weisberg *et al*, 2006; Hotamisligil & Erbay, 2008; Brestoff & Artis, 2015). Diabetes-associated inflammation also occurs in the heart, which similarly to the kidney develops interstitial fibrosis in diabetic subjects (Bugger & Abel, 2014). Indeed, it has been shown that LKB1 deletion in the heart promotes fibrosis and heart failure (Ikeda *et al*, 2009). A further setting where the link between LKB1 and inflammation may play a role is malignant disease: Somatic loss of LKB1 occurs in a variety of cancers, particularly cervical and lung cancer, which both carry a poor prognosis (Ji

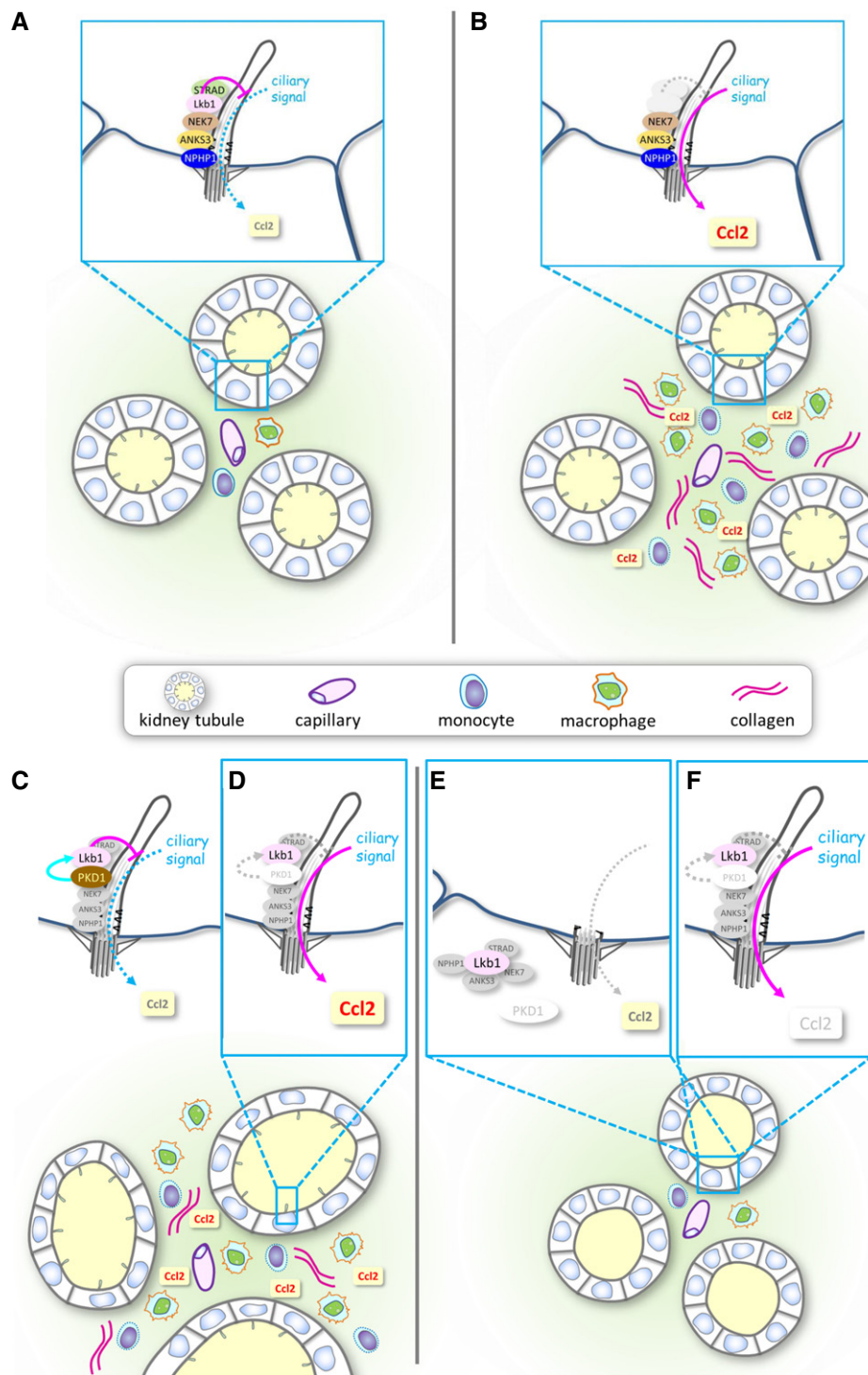


Figure 8. Graphic summary.

- A Under normal conditions, NPHP1, ANK53, NEK7, LKB1, and STRAD constitute a module within the cilium to inhibit a ciliary signal on CCL2.
- B In the absence of LKB1 or STRAD, the block is released and a ciliary signal activates expression of CCL2. This leads to the recruitment of monocytes and macrophages expressing CCR2, the CCL2 receptor; remodeling; and fibrosis.
- C PKD1 interacts with LKB1 and STRAD to activate the repressive function of the LKB1 module.
- D Loss of PKD1 results in de-repression of CCL2 expression by the module. This leads to the recruitment of monocytes and CCR2⁺ macrophages enhancing cyst growth.
- E In the absence of cilia and PKD1, the ciliary CCL2 signal cannot be activated. The recruitment of mononuclear cells is inhibited, and less cyst growth occurs.
- F Simultaneous targeting of PKD1 and CCL2 prevents the activation of mononuclear cells and ameliorates cyst growth.

et al, 2007; Wingo *et al*, 2009). It is interesting in this respect that CCL2-induced macrophage recruitment has been found to promote metastatic seeding of cancer cells (Qian *et al*, 2011; Pena *et al*, 2015) and that in pancreatic cancer, the presence of cilia correlates with more metastases and a worse prognosis (Emoto *et al*, 2014).

In summary, we describe that cilia actively promote chemokine signaling and inflammation in the kidney and that this pathway is suppressed by a module involving LKB1, NPHP-associated proteins, and PKD1. Loss of PKD1 activates the pathway and promotes disease progression in an orthologous model of ADPKD.

Materials and Methods

Mice

All animal experiments were conducted according to the guidelines of the National Institutes of Health Guide for the Care and Use of Laboratory Animals, as well as the German law for the welfare of animals, and were approved by regional authorities (Regierungspräsidentium Freiburg G-13/18, G-15/58, and G-16/28). Mice were housed in a specific pathogen-free facility, fed *ad libitum*, and housed at constant ambient temperature in a 12-hour day/night cycle. Breeding and genotyping were done according to standard procedures.

Lkb1^{flox/flox} mice (mixed genetic background) were purchased from The Jackson Laboratories (STOCK *Stk11*^{tm1.15^{jm}}/J, stock number: 014143) and were crossed to *KspCre* mice (B6.Cg-Tg (Cdh16-cre)911gr/J; C57BL/6N background; Shao *et al*, 2002) to generate a tubule-specific *Lkb1* knockout (further referred to as *Lkb1*^{ΔTub}). *Lkb1*^{flox/+} and *Lkb1*^{flox/flox} littermates without the *KspCre* transgene were used as controls. Experiments were conducted on both females and males.

For co-immunoprecipitation studies, C57BL/6J male mice were used from the local stock of the animal facility of Freiburg University.

Pkd1^{flox/flox} mice (B6.129S4-Pkd1tm2Ggg/J, stock number: 010671, C57BL/6 genetic background) and *Ccl2*-RFP^{flox/flox} (B6.Cg-Ccl2tm1.1Pame/J, stock number: 016849, C57BL/6 genetic background) were purchased from The Jackson Laboratories, and *Kif3a*^{flox/flox} mice (Kif3atm1Gsn, C57BL/6 genetic background) were kindly provided by Peter Igarashi and were crossed to *Pax8rtTA* (Traykova-Brauch *et al*, 2008) and *TetOCre* (Eremina *et al*, 2008) mice to generate an inducible tubule-specific *Pkd1* knockout (further referred to as *iPkd1*^{ΔTub}), *Pkd1*;*Ccl2* knockout (further referred to as *iPkd1*^{ΔTub};*iCcl2*^{ΔTub}), and *Pkd1*;*Kif3a* knockout (further referred to as *iPkd1*^{ΔTub};*iKif3a*^{ΔTub}). From post-natal day 28 (P28) to P42, mice received doxycycline hydrochloride (Fagron) via the drinking water (2 mg/ml with 5% sucrose, protected from light) for a period of 14 days. Littermates (lacking either TetOCre or Pax8rtTA) were used as controls. Experiments were conducted on males.

Zebrafish line maintenance and embryo manipulation

Zebrafish strains were maintained and raised as described (Epting *et al*, 2015). Transgenic *wt1b::GFP* zebrafish embryos (Perner *et al*, 2007) were injected with 0.5 mM morpholino (MO; Gene Tools LLC) targeting *lkb1* (5'-GAGATCCGCGCCACGCTCATCTTT-3' as

described; Jacob *et al*, 2011) or *nphp1* (5'-CCCTCTTCTCTTT GGAGGCATGTTG-3' as described; Slanchev *et al*, 2011) at the one-cell stage. All MOs were co-injected with 0.1 mM p53 MO (5'-GCGCCATTGCTTTGCAAGAATTG-3') to reduce the unspecific effects of the reagents. To correct for the amount of total MO in the combined knockdown experiment, 0.5 mM standard control MO (5'-CCTCTTACCTCAGTTACAATTTATA-3') was simultaneously injected. Embryos were analyzed at 48–50 h.p.f. under a Leica MZ16 stereo microscope (Leica). Images were recorded using a Leica DFC450 C (Leica).

Magnetic resonance imaging

Magnetic resonance imaging was performed on anesthetized animals at 10 and 16 weeks of age using a 9.4-T (400 MHz) horizontal magnet equipped with a 38-mm-inner-diameter quadrature birdcage coil (Bruker Biospin), as previously described (Grahammer *et al*, 2014). Briefly, anesthesia was induced with isoflurane, and breathing and heart rate were monitored by ECG. Fast imaging technique and cardiac gating were applied to reduce motion artifacts. A fast spin-echo sequence (TR/TEeff/FA: 4,800 ms/36 ms/180°; echo train length, 8) was used to achieve T2 contrast. The sequence featured a 30 × 30 mm field of view, a matrix size of 256 × 256 pixels, and an in-plane resolution of 117 × 117 mm. The slice thickness was 0.5 mm with no slice spacing to achieve contiguous image sets of the whole volume. Morphological analyses were performed using Medical Image Processing and Visualization (MIPAV) software (National Institutes of Health). To determine the total kidney volume, the perimeter of the kidney, which could be clearly distinguished from the surrounded tissue, was delineated manually on each slice image. The total kidney volume was calculated from sets of contiguous images by summing up the products of area measurements and slice thickness using the volume of interest tool in MIPAV as previously described (Grahammer *et al*, 2014).

Urine and plasma analyses

Eight-hour urine samples were obtained from mice housed in individual boxes without access to water and food. Body weight and urine excretion were measured. Urine osmolality was measured with a freezing point depression osmometer (Micro-Osmometer from Knauer or OSMOMAT 3000 basic from Gonotec). Retro-orbital blood was collected from anesthetized mice. Plasma blood urea nitrogen (BUN) was measured using urea kit (LT-UR; Labor&Technik, Eberhard Lehmann GmbH) according to the manufacturer's instructions.

Transmission electron microscopy

Transmission electron microscopy was performed as previously described (Grahammer *et al*, 2014). Briefly, 4% paraformaldehyde perfusion-fixed kidneys were post-fixed in 1% glutaraldehyde/4% paraformaldehyde for 24 h at 4°C. Subsequently, kidneys were post-fixed in 1% osmium tetroxide (Roth) for 1 h and then with 1% uranyl acetate in 70% EtOH overnight at 4°C (Polysciences), dehydrated, and embedded in Durcupan resin (Plano). Ultrathin sections were performed using a UC6 ultramicrotome (Leica), collected on

Formvar (Plano)-coated copper grids, and imaged using a Philips CM 100 transmission electron microscope.

Scanning electron microscopy

For scanning electron microscopy, 4% paraformaldehyde perfusion-fixed kidneys were post-fixed in 1% glutaraldehyde/4% paraformaldehyde for 24 h at 4°C and were subsequently dehydrated in ethanol (70–100%—each step for 1 h at RT). Dehydrated kidney samples were then incubated with the solvent HMDS in a 1:1 solution with EtOH for 30 min. The final dehydration was then performed in 100% HMDS. Kidney samples were dissected using syringe needles under a binocular microscope. Sputtering with gold was performed using a Polaron Cool Sputter Coater E 5100. Samples were visualized using a scanning electron microscope (Leo 1450 VP scanning).

Morphological analysis

Mouse kidneys were fixed in 4% paraformaldehyde and embedded in paraffin, and 4- μ m sections were stained with periodic acid–Schiff (PAS) or Picrosirius Red. PAS-stained sections were imaged using an AxioPlan2 (Zeiss) equipped with a Plan Neofluar 20 \times /0.30 NA objective and an AxioCam camera (Zeiss). PAS-stained full-size images were recorded using an AxioObserver Z1 (Zeiss) equipped with an EC Plan Neofluar 2.5 \times /0.085 NA objective and an AxioCam camera (Zeiss) or using a whole slide scanner, Nanozoomer 2.0 (Hamamatsu), equipped with a 20 \times /0.75 NA objective coupled to NDPview software (Hamamatsu). Picrosirius Red-stained sections were imaged using an AxioImager Z1 (Zeiss) equipped with a Plan Apochromat 40 \times /0.95 NA objective and an AxioCam camera (Zeiss). Image recording was performed using AxioVision software (Zeiss) or ZenBlue Software (Zeiss).

Plasmids

Tagged constructs for CD2AP, GFP, NPHP1, NPHP2, NPHP3, NPHP4, and NPHP8 were previously described (Hoff *et al*, 2013). Tagged LKB1 and STRADa constructs were kindly provided by Andrea Thiele from Hubrecht Lab and Clevers Lab, respectively. STRADb was cloned from Clone 3549243 (BioScience). FLAG.MO25a and FLAG.MO25b were cloned from canine cDNA into pcDNA6 in-frame with N-terminal FLAG tag. FLAG.PKD1 construct was kindly provided by Michael Caplan (Grimm *et al*, 2003). Flag.LKB1 for rescue experiment was cloned from human cDNA into pLXSN in-frame with Flag tag. YFP.LKB1, STRADa.YFP, and STRADb.YFP were cloned from human cDNA into pLXSN in-frame with N-terminal (LKB1) or C-terminal (STRAD constructs) YFP variant. The primers used for cloning are listed in Appendix Table S1.

Cell culture, transfections, co-immunoprecipitation, and transgenic cell lines

Human embryonic kidney (HEK 293T) cells (ATCC Promocell; CRL-11268) are listed in the database of commonly misidentified cell lines maintained by ICLAC and NCBI Biosample and were authenticated by Interspecies Determination (Isoenzyme Analysis and STR Analysis) by the providing company. HEK 293T cells were cultured using

Dulbecco's modified Eagle's medium supplemented with 10% fetal bovine serum (Biochrom). Plasmids were transiently transfected using calcium. For co-immunoprecipitation, cells were lysed in CHAPS buffer (40 mM HEPES pH 7.5, 120 mM NaCl, 1 mM EDTA, 0.30% CHAPS) supplemented with 1 mM Na₃VO₄, 50 mM NaF, 5 mM β -glycerophosphate, and protease inhibitor cocktail tablet (Roche) using a 20-G needle. Equal amounts of protein were incubated with anti-V5-agarose (Abcam, ab12229) or anti-FLAG M2 affinity gel (Sigma-Aldrich, A2220) and processed by Western blotting.

Madin-Darby canine kidney (MDCK, kind gift from Prof. Kai Simons, MPI-CBG, Dresden, Germany) cells were cultured using Dulbecco's modified Eagle's medium supplemented with 10% fetal bovine serum and 1% penicillin–streptomycin (Sigma). To generate MDCK cell lines for tetracycline-inducible knockdown of target genes, a lentivirus-based transduction system (pLVTH) was used as previously described (Wiznerowicz & Trono, 2003). The shRNA targeting sequences used were as follows: *Anks3-i1* (5'-GGAAGATGACCTCTGCCATTG-3'), *Anks3-i2* (5'-GGAGGATCGAGTCCAGGAAAT-3'), *Ift88-i* (5'-GAAGGCAGCTGAATTCTAT-3'), *Kif3a-i* (5'-AGGC TAGAGCTGAATTAGAG-3'), *Lkb1-i1* (5'-GCTGGTGGACGTGTATAC-3'), *Lkb1-i2* (5'-GGTGGACGTGTATACAAT-3'), *Luciferase* (5'-C GTACGCGGAATACTTCGA-3'), *Nek7-i1* (5'-GAGTCATGCATAGAGATATAA-3'), *Nek7-i2* (5'-CCAGCTAATGTGTTTCATTACA-3'), *Nphp1-i* (5'-GGTTCTCAGTAGACATGTA-3'; Delous *et al*, 2009), *Nphp4-i* (5'-GCCCATCGGTGTCTACACA-3'; Delous *et al*, 2009), *Strada-i* (5'-CAAGTACAGTGTCAAGTTCT-3'), and *Stradb-i* (5'-GAACACA AGTTGAATCACTCA-3'). The efficiency of the knockdown was verified by Quantitative real-time PCR (qRT-PCR) as described below (primer list in Appendix Table S1) and/or Western blot. YFP.NPHP1-, Flag.LKB1 (rescue)-, YFP.LKB1-, STRADa.YFP-, and STRADb.YFP-expressing MDCK lines were generated with a retroviral transduction system (pLXSN) as previously described (Boehlke *et al*, 2010a). *Pkd1*-null MDCK cell lines were engineered with transcription activator-like effector nucleases (TALENs) as described (Hofherr *et al*, 2017). Loss of *Pkd1* was validated by genomic PCR and RT-PCR (primer list in Appendix Table S1). For CCL2 expression analysis, 150,000 cells/cm² were seeded with or without tetracycline (5 μ g/ml) for 6 days on polycarbonate membranes (COSTAR, 3401). Total RNAs were extracted after 5 hours of serum deprivation with or without AICAR treatment (1 mM; LC Laboratories), and qRT-PCR was performed (primer list in Appendix Table S1). For immunofluorescence experiments, 150,000 cells/cm² cells were seeded for 10 days on glass coverslip coated with polylysine with or without tetracycline stimulation. All cells were regularly tested for mycoplasma contamination and were mycoplasma-free.

Quantitative real-time PCR

Total RNAs were obtained from whole kidneys or cells using RNeasy Mini Kit (Qiagen) and reverse-transcribed using SuperScript III First-Strand Synthesis SuperMix for qRT-PCR (Invitrogen) according to the manufacturer's protocol. qRT-PCR was performed on a LightCycler 480 (LC 480, Roche). *Gapdh*, *Sdha*, *Hprt*, and/or *Rpl13* were used as the normalization controls (Vandesompele *et al*, 2002). Each biological replicate was measured in technical duplicates. The primers used for qRT-PCR are listed in Appendix Table S1.

Western blot

Fresh kidney medulla was homogenized in lysis buffer (50 mM Tris pH 8, 200 mM NaCl, 1 mM EDTA, 1 mM EGTA, 1 mM DTT, 1% SDS) or CHAPS lysis buffer using a Dounce homogenizer. MDCK cells were lysed in RIPA buffer (20 mM Tris pH 8, 160 mM NaCl, 1 mM EDTA, 1 mM EGTA, 1 mM DTT, 0.1% SDS, 1% NP-40, 1% Na deoxycholate, 1% Triton X-100) using a 20-G needle. Lysis buffers were supplemented with 1 mM Na₃VO₄, 50 mM NaF, 5 mM β-glycerophosphate, and protease inhibitor cocktail tablet (Roche). Protein content was determined with Pierce BCA protein assay kit (Thermo Fisher Scientific). Equal amounts of protein were resolved on 4–15% Mini-PROTEAN TGX™ Gel (Bio-Rad) under reducing conditions, transferred, incubated with primary and secondary antibodies, and visualized on film according to standard protocols. Band density was calculated and normalized using LabImage 1D L340 software.

CCL2 ELISA

For CCL2 measurement, 150,000 MDCK cells/cm² were seeded with or without tetracycline (5 μg/ml) for 8 days on polycarbonate membranes (COSTAR, 3401). Cell culture supernatants were collected after 24 hours of serum deprivation, and particulates were removed by centrifugation. Canine CCL2 was measured using ELISA (Canine CCL2/MCP-1 Quantikine ELISA kit, R&D Systems, CACP00). Specimens, standards, and reagents were prepared according to the manufacturer's instructions.

Immunohistochemistry

Four-micrometer sections of paraffin-embedded kidneys were submitted to antigen retrieval and avidin/biotin blocking (Vector, SP-2001). Sections were incubated with primary antibody followed by biotinylated antibody, HRP-labeled streptavidin (Southern Biotech, 7100-05, 1:500), and 3,3'-diaminobenzidine-tetrahydrochloride (DAB) revelation. Images were recorded as described above.

Immunofluorescence

Four-micrometer sections of paraffin-embedded kidneys, or cells seeded on glass coverslip coated with polylysine (Sigma) were submitted to antigen retrieval and avidin/biotin blocking or cell permeabilization. The sections or coverslips were incubated with primary antibody and subsequently with the Alexa Fluor-conjugated secondary antibodies or rhodamine-labeled Dolichos Biflorus Agglutinin (DBA, Vector Laboratories, RL-1032, 1:100). Images were recorded using an Axiovert 200 M (Zeiss) and AxioVision software (Zeiss). Confocal imaging was performed on an LSM 510 Duo microscope (ZEISS) using ZenBlack Software (Zeiss).

Flow cytometry and cell sorting

After perfusion with 10 ml cold, sterile PBS, kidneys from 10-week-old *Lkb1*^{ΔTub} mice and littermate controls or 12-week-old *iPkd1*^{ΔTub} mice, *iPkd1*^{ΔTub}; *iKif3a*^{ΔTub} mice, and littermate controls were harvested, de-capsulated, minced with fine scissors, placed into a mixture of collagenase D (Worthington Biochemical) and DNase I (Roche), and shaken at 37°C for 35 min, as previously described

(Triantafyllopoulou *et al*, 2010). The cell suspension was centrifuged at 500 g for 6 min at 4°C. Cells were then triturated through nylon mesh to obtain single-cell suspensions and stained with primary antibody, DAPI (Molecular Probes) followed by Streptavidin V500 (BD Horizon) to label biotinylated antibodies. Flow cytometry was performed using a BD LSR Fortessa cytometer (BD Biosciences), and the results were analyzed with FlowJo software (TreeStar).

Mass spectrometry

Kidneys from 15-week-old C57BL/6J male mice ($n = 6$) were perfused with ice-cold PBS supplemented with 1 mM Na₃VO₄, 50 mM NaF, 5 mM β-glycerophosphate, and protease inhibitor cocktail tablet (Roche) and the medulla separated from the cortex and homogenized in CHAPS lysis buffer as described above. After lysate pre-clearing with protein G-conjugated Sepharose beads (GE Healthcare), 10 mg was incubated on a rotating wheel for 2 h at 4°C with 50 μg antibody. Protein G-conjugated Sepharose beads were added and incubated on a rotating wheel for 1 h at 4°C. The beads were collected by centrifugation and washed five times with CHAPS lysis buffer. Protein was eluted by heating in 2× Laemmli buffer containing 100 mM DTT followed by alkylation using 120 mM iodoacetamide for 20 min at 20°C in the dark. Protein mixtures were separated by SDS-PAGE (4–12% Bis-Tris mini gradient gel) and the lanes cut into five equal slices and in-gel digested with trypsin. The resulting peptide mixtures were processed on STAGE tips (Rappsilber *et al*, 2007). Three independent biological replicates were analyzed. Samples were measured on LTQ Orbitrap XL mass spectrometer (Thermo Fisher Scientific) coupled either to an Agilent 1200 nanoflow HPLC (Agilent Technologies GmbH) or to an Eksigent NanoLC Ultra. HPLC-column tips (fused silica) with 75 μm inner diameter were self-packed with Reprosil-Pur 120 ODS-3 to a length of 20 cm. No pre-column was used. Peptides were injected at a flow of 500 nl/min in 92% buffer A (0.5% acetic acid in HPLC gradient-grade water) and 2% buffer B (0.5% acetic acid in 80% acetonitrile, 20% water). Separation was achieved by a linear gradient from 10% to 30% of buffer B at a flow rate of 250 nl/min. The mass spectrometer was operated in the data-dependent mode and switched automatically between Mass spectrometry (MS) (max. of 1 × 10 ions) and MS/MS. Each MS scan was followed by a maximum of five MS/MS scans in the linear ion trap using normalized collision energy of 35% and a target value of 5,000. Parent ions with a charge state of $z = 1$ and unassigned charge states were excluded from fragmentation. The mass range for MS was $m/z = 370$ to 2,000. The resolution was set to 60,000. MS parameters were as follows: spray voltage 2.3 kV; no sheath and auxiliary gas flow; and ion transfer tube temperature 125°C.

MS data analysis

The MS raw data files were uploaded into the MaxQuant software version 1.4.1.2 (Cox & Mann, 2008), which performs peak detection and generates peak lists of mass error-corrected peptides and database searches. A full-length mouse database containing common contaminants, such as keratins and enzymes used for in-gel digestion (based on IPI human version 3.68), was employed, carbamidomethylcysteine was set as fixed modification, and methionine oxidation and protein amino-terminal acetylation were set as variable modifications. Three miss cleavages were allowed,

enzyme specificity was trypsin/P, and the MS/MS tolerance was set to 0.5 Da. The average mass precision of identified peptides was in general < 1 ppm after recalibration. Peptide lists were further used by MaxQuant to identify and relatively quantify proteins using the following parameters: peptide; and protein false discovery rates (FDR) were set to 0.01; maximum peptide posterior error probability (PEP) was set to 0.1; minimum peptide length was set to 6; minimum number peptides for identification and quantification of proteins was set to 1, which at least was unique; and identified proteins have been re-quantified.

Antibodies

Antibodies were used against the following:

For Western blotting: AMPK α (Cell Signaling Technology, 2532, 1:1,000), ANKS3 (Eurogentec, rabbit polyclonal, directed against mouse ANKS3 556–656, 1:1,000), α -TUBULIN (Sigma, T5168, 1:20,000), β -ACTIN (Sigma, A1978, 1:60,000), FLAG (M2 clone, Sigma, F-3165, 1:6,000), IFT88 (ProteinTech, 13967-1-AP, 1:1,000), KIF3a (BD Transduction, 611508, 1:1,000), LKB1 (D60C5F10, Cell Signaling Technology, 13031, 1:6,000), NEK7 (Santa Cruz Biotechnology, sc-50756 and sc-393539, 1:1,000), NPHP1 (rabbit polyclonal, kind gift from Prof. Bernhard Schermer, Köln, 1:4,000), pAMPK α ^{T172} (Cell Signaling Technology, 2535, 1:1,000), PKD1 (7E12, Santa Cruz Biotechnology, sc-130554, 1:200), pS6RP^{S235/236} (Cell Signaling Technology, 4858, 1:2,000), pTSC2^{S1387} (Cell Signaling Technology, 5584, 1:1,000), S6RP (Cell Signaling Technology, 2217, 1:1,000), TSC2 (Cell Signaling Technology, 4302, 1:1,000), and V5 (AbD Serotec, MCA1360, 1:5,000).

For immunostaining on kidney sections or MDCK cells: acetyl-alpha-tubulin (Lys40) (D20G3, Cell Signaling Technology, 5335, 1:100), acetylated tubulin (Sigma, T6793, 1:250), ANKS3 (for kidney sections: Eurogentec, rabbit polyclonal, directed against mouse ANKS3 290-395, 4 μ g/mL; and for MDCK cells: Novus Biologicals, NB100-61625, 1:100), AQP1 (Santa Cruz Biotechnology, sc-20810, 1:500), AQP2 (Santa Cruz Biotechnology, sc-9882, 1:500), F4/80 (Clone Cl:A3-1, Bio-Rad, MCA497R, 1:100), GFP (Abcam, ab13970, 1:400), IgG (Santa Cruz Biotechnology, sc-2027, 4 μ g/ml), LKB1 (D60C5F10, Cell Signaling Technology, 13031, 1:1,000 for kidney section, 1:100 for MDCK cells), pAMPK α ^{T172} (Cell Signaling Technology, 2535, 1:100), pS6RP^{S235/236} (Cell Signaling Technology, 4858, 1:100), and THP (Serotec, 8595-0054, 1:500).

For flow cytometry: The following antibodies were used: CD45 (30-F11), B220 (RA3-6B2), CD3 (145-2C11), CD19 (MB19-1), CD5 (53-7.3), CD11b (M1/70) (all from eBioscience), NK1.1 (PK136; BD Pharmingen), Ly6G (1A8; BD Bioscience), F4/80 (Bio-Rad), and CCR2 (48607; R&D Systems).

For immunoprecipitation assay: goat anti-LKB1 (M-18, Santa Cruz Biotechnology, sc-5640) and goat IgG (Santa Cruz Biotechnology, sc-2028).

Mouse microarray gene expression

Total RNAs were extracted and purified from 5-week-old control and *Lkb1*^{ATub} kidneys (five mice per genotype), using RNeasy Mini Kit (Qiagen) according to the manufacturer's protocol. RNA quality was checked using a Fragment AnalyzerTM (Advanced Analytical Technologies). cDNAs were generated and hybridized

on Affymetrix GeneChip[®] Mouse Transcriptome Arrays 1.0 according to the GeneChip[®] WT Plus assay protocol. Arrays were normalized using the Robust Multichip Algorithm (RMA) and mapped to transcript clusters using the R Bioconductor packages oligo (version 1.36.1; Carvalho & Irizarry, 2010) and mta10sttranscriptcluster.db (version 8.4). Downstream analysis considered only Entrez-annotated transcripts. If multiple transcripts mapped to the same Entrez ID, the one with the largest interquartile range between samples was chosen.

RNAseq gene expression in MDCK cells

Total RNA was obtained and verified as described above from MDCK cells with and without tetracycline-induced knockdown of LKB1 (two independent experiments per condition). Sequencing of fragmented cDNA was carried out on a HiSeq 2500 instrument (Illumina) at GATC Biotech Laboratory (Konstanz, Germany). The 50-bp paired-end reads were pseudo-aligned to the dog transcriptome (CanFam3.1) and quantified using kallisto (Bray *et al*, 2016). Downstream analysis considered only Entrez-annotated transcripts.

Microarray and RNAseq data analysis

Principal component analysis was done using the R labdsv package (version 1.8). Counts from the RNAseq data were log₂-transformed prior to analysis, and only the 1,000 most varying transcripts were considered. Differential gene expression was calculated using limma (Ritchie *et al*, 2015) and sleuth (Pimentel *et al*, 2017) for the mouse microarray and dog RNAseq data, respectively, using $q < 0.05$ as significance cutoff. Functional enrichment of differentially regulated genes was calculated from a conditional hypergeometric test as implemented in the R Bioconductor GOstats package (Falcon & Gentleman, 2007) ($P < 0.05$), and semantic similarity among GO terms was measured via the GOSemSim package (Yu *et al*, 2010).

Statistical analysis

Data were expressed as means or as means \pm SD. Differences between the experimental groups were evaluated using one-way ANOVA, followed when significant ($P < 0.05$) by the Tukey–Kramer test. When only two groups were compared, two-tailed paired *t*-test or the Mann–Whitney test was used as appropriate. For Kaplan–Meier survival curves, log-rank test was applied. The statistical analysis was performed using GraphPad Prism V6 software. For cell culture, the normal distribution of experiment replicates was systematically assumed. For animal studies, the aspect of the distribution was used to assume or not the normal distribution. Differences in variance were determined when multiple groups were compared by ANOVA. The sample size of mice was predetermined by a biostatistician. No samples were excluded from analysis. All image analyses (immunohistochemistry, immunofluorescence, MRI, FACS immunophenotyping) and mouse phenotypic analysis were performed in a blinded fashion.

Data availability

Microarray data and RNAseq data have been deposited at GEO and are available under the ID GSE86011.

Expanded View for this article is available online.

Acknowledgements

We thank Barbara Joch and Temel Kilic for technical assistance and Prof. David Bennett for critical appraisal of the manuscript. We thank the histology facility (S.F.R. Necker INSERM US24, Paris, France) for technical assistance and the ARC Foundation for funding the whole slide scanner. The grant support received was as follows: Amandine Viau: ERA-EDTA ALTF 84-2011 and FRM ARF20150934110; Frank Bienaimé: EMBO ALTF 927-2013; E. Wolfgang Kuehn: Else Kröner-Fresenius-Stiftung 2011_A87 and Deutsche Forschungsgemeinschaft KFO 201, KU 1504/5-1, 1504/7-1 and SFB1140; Melanie Boerries and Hauke Busch: Deutsche Forschungsgemeinschaft SFB850; Antogni Triantafyllopoulou: Deutsche Forschungsgemeinschaft SFB1160; Tobias B. Huber: Deutsche Forschungsgemeinschaft CRC1140, CRC 992, HU 1016/8-1 and Heisenberg program, BMBF (01GM1518C), European Research Council (ERC) Grant 616891, and H2020-IMI2 consortium BEAt-DKD; Michael Köttgen: SFB 1140 and SFB 152; Hauke Busch: Deutsche Forschungsgemeinschaft EXC306/2; and Melanie Boerries: German Federal Ministry of Education and Research (BMBF) FKZ 01ZX1409B.

Author contributions

Conceptualization: AV, FB, EWK; methodology: AV, FB, KL, SB, DP, RN, AH; investigation: AV, FB, KL, APT, MK, TAY, OK, MH, SB, TA, AM, VID; validation: M-CG; formal analysis: WR, HB, MB; resources: WR, DP, RN, FT, JD, FG, MK, GW, AT; supervision: TBH, JD, GW, AT, EWK; writing: AV, FB, HB, MB, GW, AT, MK, EWK; and funding acquisition: AV, FB, EWK.

Conflict of interest

The authors declare that they have no conflict of interest.

References

- Baas AF, Boudeau J, Sapkota GP, Smit L, Medema R, Morrice NA, Alessi DR, Clevers HC (2003) Activation of the tumour suppressor kinase LKB1 by the STE20-like pseudokinase STRAD. *EMBO J* 22: 3062–3072
- Bangs F, Anderson KV (2017) Primary cilia and mammalian hedgehog signaling. *Cold Spring Harb Perspect Biol* 9: a028175
- Boehlke C, Bashkurov M, Buescher A, Krick T, John AK, Nitschke R, Walz G, Kuehn EW (2010a) Differential role of Rab proteins in ciliary trafficking: Rab23 regulates smoothed levels. *J Cell Sci* 123: 1460–1467
- Boehlke C, Kotsis F, Patel V, Braeg S, Voelker H, Bredt S, Beyer T, Janusch H, Hamann C, Godel M, Muller K, Herbst M, Hornung M, Doerken M, Kottgen M, Nitschke R, Igarashi P, Walz G, Kuehn EW (2010b) Primary cilia regulate mTORC1 activity and cell size through Lkb1. *Nat Cell Biol* 12: 1115–1122
- Bot I, Ortiz Zacarias NV, de Witte WE, de Vries H, van Santbrink PJ, van der Velden D, Kroner MJ, van der Berg DJ, Stamos D, de Lange EC, Kuiper J, AP IJ, Heitman LH (2017) A novel CCR2 antagonist inhibits atherogenesis in apoE deficient mice by achieving high receptor occupancy. *Sci Rep* 7: 52.
- Boudeau J, Baas AF, Deak M, Morrice NA, Kieloch A, Schutkowski M, Prescott AR, Clevers HC, Alessi DR (2003) MO25alpha/beta interact with STRADalpha/beta enhancing their ability to bind, activate and localize LKB1 in the cytoplasm. *EMBO J* 22: 5102–5114
- Braun DA, Hildebrandt F (2016) Ciliopathies. *Cold Spring Harb Perspect Biol* 9: a028191
- Bray NL, Pimentel H, Melsted P, Pachter L (2016) Near-optimal probabilistic RNA-seq quantification. *Nat Biotechnol* 34: 525–527
- Brestoff JR, Artis D (2015) Immune regulation of metabolic homeostasis in health and disease. *Cell* 161: 146–160
- Bugger H, Abel ED (2014) Molecular mechanisms of diabetic cardiomyopathy. *Diabetologia* 57: 660–671
- Cao Q, Harris DC, Wang Y (2015) Macrophages in kidney injury, inflammation, and fibrosis. *Physiology (Bethesda)* 30: 183–194
- Carvalho BS, Irizarry RA (2010) A framework for oligonucleotide microarray preprocessing. *Bioinformatics* 26: 2363–2367
- Chaki M, Airik R, Ghosh AK, Giles RH, Chen R, Slaats GG, Wang H, Hurd TW, Zhou W, Cluckey A, Gee HY, Ramaswami G, Hong CJ, Hamilton BA, Cervenka I, Ganji RS, Bryja V, Arts HH, van Reeuwijk J, Oud MM et al (2012) Exome capture reveals ZNF423 and CEP164 mutations, linking renal ciliopathies to DNA damage response signaling. *Cell* 150: 533–548
- Chen L, Zhou X, Fan LX, Yao Y, Swenson-Fields KI, Gadjeva M, Wallace DP, Peters DJ, Yu A, Grantham JJ, Li X (2015) Macrophage migration inhibitory factor promotes cyst growth in polycystic kidney disease. *J Clin Invest* 125: 2399–2412
- Corbit KC, Aanstad P, Singla V, Norman AR, Stainier DY, Reiter JF (2005) Vertebrate Smoothed functions at the primary cilium. *Nature* 437: 1018–1021
- Cowley BD Jr, Ricardo SD, Nagao S, Diamond JR (2001) Increased renal expression of monocyte chemoattractant protein-1 and osteopontin in ADPKD in rats. *Kidney Int* 60: 2087–2096
- Cox J, Mann M (2008) MaxQuant enables high peptide identification rates, individualized ppb-range mass accuracies and proteome-wide protein quantification. *Nat Biotechnol* 26: 1367–1372
- Delous M, Hellman NE, Gaude HM, Silbermann F, Le Bivic A, Salomon R, Antignac C, Saunier S (2009) Nephrocystin-1 and nephrocystin-4 are required for epithelial morphogenesis and associate with PALS1/PATJ and Par6. *Hum Mol Genet* 18: 4711–4723
- Drummond IA (2012) Cilia functions in development. *Curr Opin Cell Biol* 24: 24–30
- Eckardt KU, Coresh J, Devuyst O, Johnson RJ, Kottgen A, Levey AS, Levin A (2013) Evolving importance of kidney disease: from subspecialty to global health burden. *Lancet* 382: 158–169
- Emoto K, Masugi Y, Yamazaki K, Effendi K, Tsujikawa H, Tanabe M, Kitagawa Y, Sakamoto M (2014) Presence of primary cilia in cancer cells correlates with prognosis of pancreatic ductal adenocarcinoma. *Hum Pathol* 45: 817–825
- Epting D, Slanchev K, Boehlke C, Hoff S, Loges NT, Yasunaga T, Indorf L, Nestel S, Lienkamp SS, Omran H, Kuehn EW, Ronneberger O, Walz G, Kramer-Zucker A (2015) The Rac1 regulator ELMO controls basal body migration and docking in multiciliated cells through interaction with Ezrin. *Development* 142: 174–184
- Eremina V, Jefferson JA, Kowalewska J, Hochster H, Haas M, Weisstuch J, Richardson C, Kopp JB, Kabir MG, Backx PH, Gerber HP, Ferrara N, Barisoni L, Alpers CE, Quaggin SE (2008) VEGF inhibition and renal thrombotic microangiopathy. *N Engl J Med* 358: 1129–1136
- Falcon S, Gentleman R (2007) Using GOSTats to test gene lists for GO term association. *Bioinformatics* 23: 257–258
- Franklin RA, Liao W, Sarkar A, Kim MV, Bivona MR, Liu K, Pamer EG, Li MO (2014) The cellular and molecular origin of tumor-associated macrophages. *Science* 344: 921–925
- García-González FR, Reiter JF (2017) Open sesame: how transition fibers and the transition zone control ciliary composition. *Cold Spring Harb Perspect Biol* 9: a028134
- GBD2015-Collaborators (2016) Global, regional, and national life expectancy, all-cause mortality, and cause-specific mortality for 249 causes of death,

- 1980–2015: a systematic analysis for the Global Burden of Disease Study 2015. *Lancet* 388: 1459–1544
- Grahammer F, Haenisch N, Steinhardt F, Sandner L, Roerden M, Arnold F, Cordts T, Wanner N, Reichardt W, Kerjaschki D, Ruegg MA, Hall MN, Moulin P, Busch H, Boerries M, Walz G, Artunc F, Huber TB (2014) mTORC1 maintains renal tubular homeostasis and is essential in response to ischemic stress. *Proc Natl Acad Sci USA* 111: E2817–E2826
- Grimm DH, Cai Y, Chauvet V, Rajendran V, Zeltner R, Geng L, Avner ED, Sweeney W, Somlo S, Caplan MJ (2003) Polycystin-1 distribution is modulated by polycystin-2 expression in mammalian cells. *J Biol Chem* 278: 36786–36793
- Halbritter J, Porath JD, Diaz KA, Braun DA, Kohl S, Chaki M, Allen SJ, Soliman NA, Hildebrandt F, Otto EA (2013) Identification of 99 novel mutations in a worldwide cohort of 1,056 patients with a nephronophthisis-related ciliopathy. *Hum Genet* 132: 865–884
- Han SH, Malaga-Dieguez L, Chinga F, Kang HM, Tao J, Reidy K, Susztak K (2016) Deletion of *Lkb1* in renal tubular epithelial cells leads to CKD by altering metabolism. *J Am Soc Nephrol* 27: 439–453
- Hemminki A, Markie D, Tomlinson I, Avizienyte E, Roth S, Loukola A, Bignell G, Warren W, Aminoff M, Hoglund P, Jarvinen H, Kristo P, Pelin K, Ridanpaa M, Salovaara R, Toro T, Bodmer W, Olschwang S, Olsen AS, Stratton MR et al (1998) A serine/threonine kinase gene defective in Peutz-Jeghers syndrome. *Nature* 391: 184–187
- Hildebrandt F, Otto E, Rensing C, Nothwang HG, Vollmer M, Adolphs J, Hanusch H, Brandis M (1997) A novel gene encoding an SH3 domain protein is mutated in nephronophthisis type 1. *Nat Genet* 17: 149–153
- Hildebrandt F, Benzing T, Katsanis N (2011) Ciliopathies. *N Engl J Med* 364: 1533–1543
- Hoff S, Halbritter J, Epting D, Frank V, Nguyen TM, van Reeuwijk J, Boehlke C, Schell C, Yasunaga T, Helmstadter M, Mergen M, Filhol E, Boldt K, Horn N, Ueffing M, Otto EA, Eisenberger T, Elting MW, van Wijk JA, Bockenhauer D et al (2013) ANK56 is a central component of a nephronophthisis module linking NEK8 to INVS and NPHP3. *Nat Genet* 45: 951–956
- Hofherr A, Busch T, Huber N, Nold A, Bohn A, Viau A, Bienaime F, Kuehn EW, Arnold SJ, Kottgen M (2017) Efficient genome editing of differentiated renal epithelial cells. *Pflugers Arch* 469: 303–311
- Hotamisligil GS, Erbay E (2008) Nutrient sensing and inflammation in metabolic diseases. *Nat Rev Immunol* 8: 923–934
- Ikeda Y, Sato K, Pimentel DR, Sam F, Shaw RJ, Dyck JR, Walsh K (2009) Cardiac-specific deletion of LKB1 leads to hypertrophy and dysfunction. *J Biol Chem* 284: 35839–35849
- Jacob LS, Wu X, Dodge ME, Fan CW, Kulak O, Chen B, Tang W, Wang B, Amatruda JF, Lum L (2011) Genome-wide RNAi screen reveals disease-associated genes that are common to Hedgehog and Wnt signaling. *Sci Signal* 4: ra4
- Ji H, Ramsey MR, Hayes DN, Fan C, McNamara K, Kozlowski P, Torrice C, Wu MC, Shimamura T, Perera SA, Liang MC, Cai D, Naumov GN, Bao L, Contreras CM, Li D, Chen L, Krishnamurthy J, Koivunen J, Chiriac LR et al (2007) LKB1 modulates lung cancer differentiation and metastasis. *Nature* 448: 807–810
- Jones C, Roper VC, Foucher I, Qian D, Banizs B, Petit C, Yoder BK, Chen P (2008) Ciliary proteins link basal body polarization to planar cell polarity regulation. *Nat Genet* 40: 69–77
- Karihaloo A, Koraisly F, Huen SC, Lee Y, Merrick D, Caplan MJ, Somlo S, Cantley LG (2011) Macrophages promote cyst growth in polycystic kidney disease. *J Am Soc Nephrol* 22: 1809–1814
- Kim JC, Badano JL, Sibold S, Esmail MA, Hill J, Hoskins BE, Leitch CC, Venner K, Ansley SJ, Ross AJ, Leroux MR, Katsanis N, Beales PL (2004) The Bardet-Biedl protein BBS4 targets cargo to the pericentriolar region and is required for microtubule anchoring and cell cycle progression. *Nat Genet* 36: 462–470
- Konig J, Kranz B, Konig S, Schlingmann KP, Titieni A, Tonshoff B, Habbig S, Pape L, Haffner K, Hansen M, Buscher A, Bald M, Billing H, Schild R, Walden U, Hampel T, Staude H, Riedl M, Gretz N, Lablans M et al (2017) Phenotypic spectrum of children with nephronophthisis and related ciliopathies. *Clin J Am Soc Nephrol* 12: 1974–1983
- Kramer-Zucker AG, Olale F, Haycraft CJ, Yoder BK, Schier AF, Drummond IA (2005) Cilia-driven fluid flow in the zebrafish pronephros, brain and Kupffer's vesicle is required for normal organogenesis. *Development* 132: 1907–1921
- Lechtreck KF, Johnson EC, Sakai T, Cochran D, Ballif BA, Rush J, Pazour GJ, Ikebe M, Witman GB (2009) The Chlamydomonas reinhardtii BBSome is an IFT cargo required for export of specific signaling proteins from flagella. *J Cell Biol* 187: 1117–1132
- Leetola CN, Knight MJ, Cascio D, Hoffman S, Bowie JU (2014) Characterization of the SAM domain of the PKD-related protein ANKS6 and its interaction with ANKS3. *BMC Struct Biol* 14: 17
- Liu YM, Shao YQ, He Q (2014) Sirolimus for treatment of autosomal-dominant polycystic kidney disease: a meta-analysis of randomized controlled trials. *Transpl Proc* 46: 66–74
- Lizcano JM, Goransson O, Toth R, Deak M, Morrice NA, Boudeau J, Hawley SA, Udd L, Makela TP, Hardie DG, Alessi DR (2004) LKB1 is a master kinase that activates 13 kinases of the AMPK subfamily, including MARK/PAR-1. *EMBO J* 23: 833–843
- Ma M, Tian X, Igarashi P, Pazour GJ, Somlo S (2013) Loss of cilia suppresses cyst growth in genetic models of autosomal dominant polycystic kidney disease. *Nat Genet* 45: 1004–1012
- Marszalek JR, Ruiz-Lozano P, Roberts E, Chien KR, Goldstein LS (1999) Situs inversus and embryonic ciliary morphogenesis defects in mouse mutants lacking the KIF3A subunit of kinesin-II. *Proc Natl Acad Sci USA* 96: 5043–5048
- Menezes LF, Lin CC, Zhou F, Germino GG (2016) Fatty acid oxidation is impaired in an orthologous mouse model of autosomal dominant polycystic kidney disease. *EBioMedicine* 5: 183–192
- Mick DU, Rodrigues RB, Leib RD, Adams CM, Chien AS, Gygi SP, Nachury MV (2015) Proteomics of primary cilia by proximity labeling. *Dev Cell* 35: 497–512
- Mochizuki T, Wu G, Hayashi T, Xenophontos SL, Veldhuisen B, Saris JJ, Reynolds DM, Cai Y, Gabow PA, Pierides A, Kimberling WJ, Breuning MH, Deltas CC, Peters DJ, Somlo S (1996) PKD2, a gene for polycystic kidney disease that encodes an integral membrane protein. *Science* 272: 1339–1342
- Nachury MV (2014) How do cilia organize signalling cascades?. *Philos Trans R Soc Lond B Biol Sci* 369: 20130465
- Nakada D, Saunders TL, Morrison SJ (2010) Lkb1 regulates cell cycle and energy metabolism in haematopoietic stem cells. *Nature* 468: 653–658
- Norman J (2011) Fibrosis and progression of autosomal dominant polycystic kidney disease (ADPKD). *Biochem Biophys Acta* 1812: 1327–1336
- Ong AC, Devuyt O, Knebelmann B, Walz G (2015) Autosomal dominant polycystic kidney disease: the changing face of clinical management. *Lancet* 385: 1993–2002
- Orhon I, Dupont N, Zaidan M, Boitez V, Burtin M, Schmitt A, Capiod T, Viau A, Beau I, Wolfgang Kuehn E, Friedlander G, Terzi F, Codogno P (2016) Primary-cilium-dependent autophagy controls epithelial cell volume in response to fluid flow. *Nat Cell Biol* 18: 657–667
- Park TJ, Haigo SL, Wallingford JB (2006) Ciliogenesis defects in embryos lacking returned or fuzzy function are associated with failure of planar cell polarity and Hedgehog signaling. *Nat Genet* 38: 303–311

- Pazour GJ, Dickert BL, Vucica Y, Seeley ES, Rosenbaum JL, Witman GB, Cole DG (2000) Chlamydomonas IFT88 and its mouse homologue, polycystic kidney disease gene tg737, are required for assembly of cilia and flagella. *J Cell Biol* 151: 709–718
- Pena CG, Nakada Y, Saatcioglu HD, Aloisio GM, Cuevas I, Zhang S, Miller DS, Lea JS, Wong KK, DeBerardinis RJ, Amelio AL, Brekken RA, Castrillon DH (2015) LKB1 loss promotes endometrial cancer progression via CCL2-dependent macrophage recruitment. *J Clin Invest* 125: 4063–4076
- Perner B, Englert C, Bollig F (2007) The Wilms tumor genes wt1a and wt1b control different steps during formation of the zebrafish pronephros. *Dev Biol* 309: 87–96
- Pimentel H, Bray NL, Puente S, Melsted P, Pachter L (2017) Differential analysis of RNA-seq incorporating quantification uncertainty. *Nat Methods* 14: 687–690
- Praetorius HA, Spring KR (2001) Bending the MDCK cell primary cilium increases intracellular calcium. *J Membr Biol* 184: 71–79
- Puri P, Bushnell D, Schaefer CM, Bates CM (2016) Six2creFrs2alpha knockout mice are a novel model of renal cystogenesis. *Sci Rep* 6: 36736
- Qian BZ, Li J, Zhang H, Kitamura T, Zhang J, Campion LR, Kaiser EA, Snyder LA, Pollard JW (2011) CCL2 recruits inflammatory monocytes to facilitate breast-tumour metastasis. *Nature* 475: 222–225
- Ramachandran H, Engel C, Muller B, Dengjel J, Walz G, Yakulov TA (2015) Anks3 alters the sub-cellular localization of the Nek7 kinase. *Biochem Biophys Res Comm* 464: 901–907
- Rappsilber J, Mann M, Ishihama Y (2007) Protocol for micro-purification, enrichment, pre-fractionation and storage of peptides for proteomics using StageTips. *Nat Protoc* 2: 1896–1906
- Ritchie ME, Phipson B, Wu D, Hu Y, Law CW, Shi W, Smyth GK (2015) Limma powers differential expression analyses for RNA-sequencing and microarray studies. *Nucleic Acids Res* 43: e47
- Robert A, Margall-Ducos G, Guidotti JE, Bregerie O, Celati C, Brechot C, Desdouts C (2007) The intraflagellar transport component IFT88/polaris is a centrosomal protein regulating G1-S transition in non-ciliated cells. *J Cell Sci* 120: 628–637
- Rowe I, Chiaravalli M, Mannella V, Ulisse V, Quilici G, Pema M, Song XW, Xu H, Mari S, Qian F, Pei Y, Musco G, Boletta A (2013) Defective glucose metabolism in polycystic kidney disease identifies a new therapeutic strategy. *Nat Med* 19: 488–493
- Saunier S, Calado J, Heilig R, Silbermann F, Benessy F, Morin G, Konrad M, Broyer M, Gubler MC, Weissenbach J, Antignac C (1997) A novel gene that encodes a protein with a putative src homology 3 domain is a candidate gene for familial juvenile nephronophthisis. *Hum Mol Genet* 6: 2317–2323
- Sayyed SG, Ryu M, Kulkarni OP, Schmid H, Lichtnekert J, Gruner S, Green L, Mattei P, Hartmann G, Anders HJ (2011) An orally active chemokine receptor CCR2 antagonist prevents glomerulosclerosis and renal failure in type 2 diabetes. *Kidney Int* 80: 68–78
- Schneider L, Cammer M, Lehman J, Nielsen SK, Guerra CF, Veland IR, Stock C, Hoffmann EK, Yoder BK, Schwab A, Satir P, Christensen ST (2010) Directional cell migration and chemotaxis in wound healing response to PDGF-AA are coordinated by the primary cilium in fibroblasts. *Cell Physiol Biochem* 25: 279–292
- Serbina NV, Pamer EG (2006) Monocyte emigration from bone marrow during bacterial infection requires signals mediated by chemokine receptor CCR2. *Nat Immunol* 7: 311–317
- Shamseldin HE, Yakulov TA, Hashem A, Walz G, Alkuraya FS (2016) ANKS3 is mutated in a family with autosomal recessive laterality defect. *Hum Genet* 135: 1233–1239
- Shao X, Somlo S, Igarashi P (2002) Epithelial-specific Cre/lox recombination in the developing kidney and genitourinary tract. *J Am Soc Nephrol* 13: 1837–1846
- Shaw RJ, Kosmatka M, Bardeesy N, Hurley RL, Witters LA, DePinho RA, Cantley LC (2004) The tumor suppressor LKB1 kinase directly activates AMP-activated kinase and regulates apoptosis in response to energy stress. *Proc Natl Acad Sci USA* 101: 3329–3335
- Slaats GG, Lillien MR, Giles RH (2016) Nephronophthisis: should we target cysts or fibrosis? *Pediatr Nephrol* 31: 545–554
- Slanchev K, Putz M, Schmitt A, Kramer-Zucker A, Walz G (2011) Nephrocystin-4 is required for pronephric duct-dependent cloaca formation in zebrafish. *Hum Mol Genet* 20: 3119–3128
- Stepanek L, Pigino G (2016) Microtubule doublets are double-track railways for intraflagellar transport trains. *Science* 352: 721–724
- The International Polycystic Kidney Disease Consortium (1995) Polycystic kidney disease: the complete structure of the PKD1 gene and its protein. *Cell* 81: 289–298
- Titze S, Schmid M, Kottgen A, Busch M, Floege J, Wanner C, Kronenberg F, Eckardt KU (2015) Disease burden and risk profile in referred patients with moderate chronic kidney disease: composition of the German Chronic Kidney Disease (GCKD) cohort. *Nephrol Dial Transplant* 30: 441–451
- Traykova-Brauch M, Schonig K, Greiner O, Miloud T, Jauch A, Bode M, Felsher DW, Glick AB, Kwiatkowski DJ, Bujard H, Horst J, von Knebel Doeberitz M, Niggli FK, Kriz W, Grone HJ, Koesters R (2008) An efficient and versatile system for acute and chronic modulation of renal tubular function in transgenic mice. *Nat Med* 14: 979–984
- Triantafyllopoulou A, Franzke CW, Seshan SV, Perino G, Kalliolias GD, Ramanujam M, van Rooijen N, Davidson A, Ivashkiv LB (2010) Proliferative lesions and metalloproteinase activity in murine lupus nephritis mediated by type I interferons and macrophages. *Proc Natl Acad Sci USA* 107: 3012–3017
- Tuz K, Bachmann-Gagescu R, O'Day DR, Hua K, Isabella CR, Phelps IG, Stolarski AE, O'Roak BJ, Dempsey JC, Lourenco C, Alswaid A, Bonnemann CG, Medne L, Nampoothiri S, Stark Z, Leventer RJ, Topcu M, Cansu A, Jagadeesh S, Done S et al (2014) Mutations in CSPP1 cause primary cilia abnormalities and Joubert syndrome with or without Jeune asphyxiating thoracic dystrophy. *Am J Hum Genet* 94: 62–72
- UKPDS Group (1998) Effect of intensive blood-glucose control with metformin on complications in overweight patients with type 2 diabetes (UKPDS 34). UK Prospective Diabetes Study (UKPDS) Group. *Lancet* 352: 854–865
- Vandesompele J, De Preter K, Pattyn F, Poppe B, Van Roy N, De Paepe A, Speleman F (2002) Accurate normalization of real-time quantitative RT-PCR data by geometric averaging of multiple internal control genes. *Genome Biol* 3: RESEARCH0034
- Vasilyev A, Liu Y, Mudumana S, Mangos S, Lam PY, Majumdar A, Zhao J, Poon KL, Kondrychyn I, Korzh V, Drummond IA (2009) Collective cell migration drives morphogenesis of the kidney nephron. *PLoS Biol* 7: e9
- Walz G, Budde K, Mannaa M, Nurnberger J, Wanner C, Sommerer C, Kundendorf U, Banas B, Horl WH, Obermuller N, Arns W, Pavenstadt H, Gaedeke J, Buchert M, May C, Gschaidmeier H, Kramer S, Eckardt KU (2010) Everolimus in patients with autosomal dominant polycystic kidney disease. *N Engl J Med* 363: 830–840
- Weisberg SP, Hunter D, Huber R, Lemieux J, Slaymaker S, Vaddi K, Charo I, Leibel RL, Ferrante AW Jr (2006) CCR2 modulates inflammatory and metabolic effects of high-fat feeding. *J Clin Invest* 116: 115–124

- Wingo SN, Gallardo TD, Akbay EA, Liang MC, Contreras CM, Boren T, Shimamura T, Miller DS, Sharpless NE, Bardeesy N, Kwiatkowski DJ, Schorge JO, Wong KK, Castrillon DH (2009) Somatic LKB1 mutations promote cervical cancer progression. *PLoS One* 4: e5137
- Wiznerowicz M, Trono D (2003) Conditional suppression of cellular genes: lentivirus vector-mediated drug-inducible RNA interference. *J Virol* 77: 8957–8961
- Wolf MT (2015) Nephronophthisis and related syndromes. *Curr Opin Pediatr* 27: 201–211
- Yakulov TA, Yasunaga T, Ramachandran H, Engel C, Muller B, Hoff S, Dengjel J, Lienkamp SS, Walz G (2015) Anks3 interacts with nephronophthisis proteins and is required for normal renal development. *Kidney Int* 87: 1191–1200
- Yu G, Li F, Qin Y, Bo X, Wu Y, Wang S (2010) GOSemSim: an R package for measuring semantic similarity among GO terms and gene products. *Bioinformatics* 26: 976–978
- Zeqiraj E, Filippi BM, Deak M, Alessi DR, van Aalten DM (2009) Structure of the LKB1-STRAD-MO25 complex reveals an allosteric mechanism of kinase activation. *Science* 326: 1707–1711
- Zheng D, Wolfe M, Cowley BD Jr, Wallace DP, Yamaguchi T, Grantham JJ (2003) Urinary excretion of monocyte chemoattractant protein-1 in autosomal dominant polycystic kidney disease. *J Am Soc Nephrol* 14: 2588–2595



License: This is an open access article under the terms of the Creative Commons Attribution-NonCommercial-NoDerivs 4.0 License, which permits use and distribution in any medium, provided the original work is properly cited, the use is non-commercial and no modifications or adaptations are made.